Arctic Sea Ice Extent and Anomalies, 1953-1984

Lawrence A. Mysak and Davinder K. Manak

CRG Report No. 88-8

June 1988

ARCTIC SEA ICE EXTENT AND ANOMALIES, 1953-1984

by

Lawrence A. Mysak and Davinder K. Manak

Climate Research Group

Department of Meteorology

McGill University

Montreal, Quebec H3A 2K6

June 1988

(submitted to Atmosphere-Ocean)

Abstract

A study is presented of the seasonal and interannual variability of Arctic sea ice extent over the 32-y period 1953-84. The data set used consists of monthly sea ice concentration values given on a 1° latitude grid and represents a 7-y extension of the 25-y data set analyzed by Walsh and Johnson (1979). By focussing attention on the variability in seven distinct subregions which circumscribe the polar region, a number of interesting spatial patterns emerge in the regional seasonal cycles and anomalies of ice coverage. For example, the time scale of the smoothed anomaly fluctuations varies from a 4-6 y cycle in the western Arctic (e.g., the Beaufort Sea) to a decadal one in the eastern Arctic (e.g., the Barents Sea). Also, in agreement with earlier studies, a significant out of phase relationship was found between the 25-month smoothed anomalies in the Beaufort & Chukchi Sea region and the Greenland Sea. It is proposed that this behaviour is related to atmospheric pressure anomalies associated with the seesaw in winter air temperature between northern Europe and western Greenland. Finally, a particularly large 9-y ice anomaly in the Greenland Sea, which was centered around 1968, appears to have evolved into a substantial 4-y Labrador Sea anomaly, which peaked in 1972. Both of these anomalies coincided with the passage of the "Great Salinity Anomaly", which traversed cyclonically around the subpolar gyre in the northern North Atlantic during the period 1968-82.

1. Introduction

During the past decade there have been a number of observational studies of the seasonal and interannual variability of sea ice in the Arctic (e.g., Walsh and Johnson, 1979; Lemke et al., 1980; Parkinson et al., 1987). Such analyses, which involve data sets ranging from four- to twenty-five year periods, have been used to validate the results of stochastic climate models (Lemke et al., 1980) and deterministic ice-ocean circulation models (Hibler and Bryan, 1987; Semtner, 1987; Willmott and Mysak, 1988). Also, these studies have helped us to better understand high-latitude climate processes and to answer pressing questions concerning navigation, resource development, environmental protection and fisheries in the Arctic.

The main purpose of this paper is to present an analysis of an extensive record (32 years) of monthly Arctic sea ice concentration data which has been assembled by John Walsh of the University of Illinois. This data set has been compiled from eight different sources (see §2 below) and represents a seven year extension of the 25-year (1953-77) data set analyzed by Walsh and Johnson (1979). These authors focussed on the variability of the sea ice in the Arctic basin as a whole and used empirical orthogonal functions (EOF's) of longitude to identify the major spatial and temporal scales of the ice fluctuations during the aforementioned 25-year period. In the extended data set used in this paper, we have chosen to focus on the seasonal and interannual variability of the sea ice extent in seven subregions or seas which circumscribe the polar cap (see Fig. 1 below). By proceeding in this manner we have not only confirmed vividly some of the findings of Walsh and Johnson (1979) (e.g., the

opposition of the ice anomalies in the Greenland Sea with those in the Beaufort & Chukchi Sea subregion), but also have identified new spatial structures and time scales of the ice anomaly fluctuations in the various subregions. In the light of these discoveries, a description is also given of a number of processes and mechanisms concerning air/sea and air/ice/sea interactions that may help to explain these various anomalies. Some of these processes have been discussed in general terms by Walsh (1983) and Untersteiner (1986), but they have not been related directly to the data set analyzed in this report.

The outline of this paper is as follows. The sea ice concentration data and the seven Arctic subregions are described in section 2. A general discussion of several maps of Arctic sea ice extent taken from Manak and Mysak (1987) is given in section 3. In section 4 the seasonal cycles of the areal sea ice extent in the total Arctic region as well as in the various subregions are shown, and in section 5 the ice anomalies of these regions are described. Section 6 is devoted to a discussion of a particularly significant ice anomaly that appeared during 1963-72 in the Greenland Sea.

2. Sea ice concentration data

The sea ice distribution data used in this study were compiled by John Walsh from the data sources listed in Table 1, and consist of monthly sea ice concentration grids for the years 1953-84 inclusive. Sea ice concentration is defined as the fraction of a grid area covered by ice and is given in tenths. The ice concentrations were given on a 58x80 point grid with one degree latitude (approximately 110 km) spacing (see Figure 1). The one degree spacing was chosen to permit the resolution of year-to-year fluctuations. Finer resolution was not justifiable due to the quality of the earlier data.

By using a synthesized data set, a fairly long record has been obtained which permits the identification of fluctuations of up to decadal time scales. However, it should be kept in mind that there are a number of factors (e.g., variety of observational techniques, imprecise concentration classifications, missing data) which may contribute to some nonuniformity in the synthesized data, especially in the earlier years (see Walsh and Johnson (1979) for further details).

The sea ice data were segregated into four seasons: "winter" (December, January, February), "spring" (March, April, May), "summer" (June, July, August) and "autumn" (September, October, November). The winters are labelled by the year in which they end. For example, winter 1970 refers to the period December 1969 - February 1970. A climatology for each season was constructed by averaging the seasonal data for the 32 year period, 1953-1984. The "annual climatology" was obtained by averaging the seasonal climatologies. In the recent atlas by Manak and Mysak (1987), seasonal maps of the sea ice extent (according to ice concentration) for each year of the 32-year period

are presented along with the seasonal climatological maps. In sections 3 and 6 below some of these maps are presented.

To study the spatial and temporal variability of sea ice extent and anomalies, the grid for the region of study was divided into 7 subregions, as shown in Figure 1. The names of the subregions are listed in Table 2.

Time series of monthly means and anomalies of areal sea ice extent were constructed for the total Arctic region and for each of the 7 subregions shown in Fig. 1. The monthly mean ice concentration grid values were first obtained by averaging the monthly concentration data over the 32 years (1953-84). The monthly ice concentration anomalies, for a given year, were then obtained by subtracting these monthly means from the monthly concentration values for that year. The monthly areal ice anomalies in a given region were then calculated by summing (over all the grid points in the region) the products of these monthly concentration anomalies and their corresponding ocean areas. This process removed the climatological annual cycle, leaving monthly anomalies of areal ice extent. Interannual and decadal fluctuations in the ice coverage can then be studied by looking at the time series of these monthly anomalies.

3. Sea ice extent maps

Figure 2 shows a map of the annual climatology of the sea ice extent (according to ice concentration) in the Arctic region. The ice concentration contours are labelled in tenths; thus the 1, 5, and 9 contour lines correspond to 10%, 50%, and 90% ice coverage, respectively. The 5/10 line can be taken as a rough approximation to the ice/no-ice boundary. Note that the polar region is totally frozen (> 9/10 ice concentration), and that the ice concentrations exceed 5/10 along the Siberian coast.

It has long been known that the marginal ice zone in the Arctic (roughly the area between the 1/10 and 5/10 contours in Fig. 2) marks the northern boundary of a fairly narrow band of relatively high biological productivity because the water here is generally not vertically stable (Dunbar, 1986). This region is also called the "Marine Subarctic", and represents a mixture of Arctic and non-Arctic (Atlantic or Pacific) water. Figure 3 vividly shows the close proximity of the 5/10 ice concentration contour in the North Atlantic - Labrador Sea region to the Marine Subarctic region where many important fisheries have developed over the centuries (e.g., Atlantic cod, salmon, capelin and redfish). It is thus evident that significant climatic changes which affect the position of the ice margin will have dramatic effects on the survival and/or location of these fisheries and hence on the economies of the neighbouring high-latitude countries.

Another interesting comparison that can be made with the ice climatology in Fig. 2 is the large-scale horizontal ocean circulation pattern in the north polar region (Fig. 4). Upon examining these two

figures it can be seen that the positions of the ice edges are largely determined by the surface circulation patterns associated with the subpolar gyres. For example, the high-latitude position of the 10% contour in the eastern part of the Greenland Sea and the northern part of the Barents Sea is caused by the northward transport of warm water by the Norwegian Current. Similarly the West Greenland Current and the eastern part of the Bering gyre (see Fig. 4) produce relatively ice-free regions off the southwest corner of Greenland and along the western coast of Alaska respectively. On the other hand, the southward transport of cold water by the East Greenland Current, the Labrador Current and the East Kamchatka Current produce extensive ice coverage along the east coast of Greenland, the Labrador coast and the east coast of the Kamchatka peninsula, respectively.

Figure 5 shows the climatologies of sea ice extent for each season. Comparing the winter climatology with the annual climatology (Fig. 2), it can be seen that during this season all of the ice edges have moved further out from the polar region, resulting in a much larger area of greater than 90% ice coverage. The spring climatology shows the ice cover starting to break up in Hudson Bay, Baffin Bay, and the Bering Sea. By summer, the ice extent is at its minimum and the Bering Strait and Hudson Bay are open. Also, there are open patches along the Siberian coastline. In autumn, the water starts to freeze up along the ice edges. A further discussion of this seasonal cycle will be given in section 4, along with a region by region description of the mean monthly changes of areal sea ice extent. Next, however, we wish to describe two particularly interesting sets of sea ice extent maps taken from the atlas of Manak and Mysak (1987).

Figure 6 shows two contrasting situations for the autumn sea ice extent in the Beaufort gyre region (see Fig. 4). Upon comparing the upper part of Fig. 6 with the autumn climatology in Fig. 5, we observe that the Beaufort & Chukchi Sea region (subregion 2 in Fig. 1) had considerably less ice than normal during autumn 1982. This may be due to the presence of a very strong high pressure system over the Beaufort Sea during September 1982 (Ross and Walsh, 1988), which would have produced ice convergence (via Ekman transport) toward the centre of this high pressure cell and resulted in less ice off the northern coast of Alaska and Canada. On the other hand, the severe ice conditions in this same region during autumn 1983 (Fig. 6, lower panel) were most likely caused by the existence of an anomalous low pressure system over the Beaufort Sea during September 1983 (Ross and Walsh, 1988) which would produce ice divergence away from the centre of the low and also a reversal of the Beaufort gyre (McLaren et al., 1988).

The four year sequence of winter maps in Fig. 7 shows a progression of states from relatively low ice concentrations in parts of Hudson Bay (subregion 3) and the Baffin Bay/Labrador Sea region (subregion 4) to rather large ice concentrations. Following a year of typical weather and ice conditions in subregions 3 and 4 during 1980 (Manak and Mysak, 1987), the winter of 1981 was very mild, with the 9/10 ice concentration contour extending northward well into Baffin Bay. Also evident in Fig. 7 are a large number of polynyas (open patches of water) around the perimeter of Hudson Bay and the "North Water", a famous polynya at the head of Baffin Bay (Dunbar, 1986). However, during winter 1983 these polynyas were absent, and much of

the Labrador Sea was ice covered. Also, there was considerable sea ice off the east coast of Newfoundland. These severe conditions also occurred in winter 1984 (Fig. 7, lower right panel) and have been observed by Parkinson and Cavalieri (1988) using passive microwave satellite measurements. It is proposed here that the above severe ice conditions during winter 1983 were due to anomalous atmospheric forcing associated with the very strong 1982-83 El Niño/Southern Oscillation (ENSO) event. Figure 8 shows the Pacific North American (PNA) teleconnection patterns associated with a typical ENSO event (left side) and the extraordinary 1982-83 ENSO event, which was the strongest of the century. Of particular interest to us here is the anomalously strong high pressure system associated with the 1982-83 PNA teleconnection pattern which was centered just south of Hudson Bay during winter 1983. On the northern flank of this anticyclonic system there was anomalously cold air flowing across northern Canada and down into the Labrador Sea region. We argue that it was this cold air mass which produced the anomalous ice conditions in the Labrador Sea during winter 1983. Furthermore, because of the thermal inertia associated with sea ice, these severe ice conditions persisted through to 1984 at least.

4. Seasonal cycles of sea ice extent

a. Total Arctic region

Figure 9 shows the normal seasonal cycle of the areal sea ice extent in the entire Arctic region. The data points plotted are the 32-year averages of area covered by ice at the end of each month. The strong, smooth yearly cycle is most evident; however, there is a slight delay in the melting period during the spring months, which gives rise to an asymmetry in the cycle. The maximum ice extent occurs in late February, and amounts to 14×10^6 km^2; the minimum of 7×10^6 km^2 occurs at the end of August. This seasonal variation is significant and is equivalent to about 70% of the total area of Canada! It is interesting to note that in the Southern Ocean the maximum and minimum sea ice extents are 20×10^6 km^2 and 4×10^6 km^2 respectively (Zwally et al., 1983). The results shown in Fig. 9 are consistent with those of Walsh and Johnson (1979), who used a shortened version (1953-77) of the same data set.

b. The subregions

The seasonal cycles for the Bering Sea and the Beaufort & Chukchi Seas are shown in Figure 10. The Bering Sea is totally ice-free from late June to late October. In the Beaufort Sea region the period of low ice coverage during summer is quite short and ice growth is more rapid than decay.

Figure 11 shows the seasonal cycles for regions 3 and 4. Hudson Bay is totally frozen in winter, but never completely thaws out, even in summer. The Baffin Bay/Labrador Sea region has maximum ice coverage in February, although it is never completely frozen (see Fig.

5, the map of winter climatology).

Figure 12 shows the seasonal cycles for the remaining three regions. Note that in the Greenland Sea (region 5) the amplitude of the seasonal cycle is quite small. This is because of strong current-ice edge interaction and the small amplitude of the seasonal fluctuations of the East Greenland Current. From Fig. 12 we also note that in the Barents & Kara Seas, the seasonal cycle is much greater than in the East-Siberian & Laptev Seas even though the period of low ice concentration is similar for both regions.

5. Anomalies of sea ice extent

We now focus our attention on the fluctuations of areal sea ice extent by examining various time series of the ice anomalies as defined in section 2. It will be seen that these deviations from the seasonal cycle clearly portray the structure of high-latitude climatic fluctuations on time scales of years to decades.

a. Total Arctic region

Figure 13 shows the smoothed time series of the monthly anomalies of the area covered by Arctic sea ice. To reduce the noise in the monthly anomaly time series 3-month and 25-month running means were used. Both anomaly curves are shown in Fig. 13 (and in subsequent figures, 15-21): the lighter curve is the 3-month running mean, the darker curve is the 25-month running mean. The 3-month running mean shows the year-to-year fluctuations in the Arctic sea ice extent, whereas the 25-month running mean highlights the approximate decadal cycle in the anomaly field. From the latter running mean we see that a relatively small negative ice anomaly during 1959-64 is followed by a large positive anomaly (whose maximum is about half the size of Hudson Bay) during 1965-1973 which in turn is followed by a negative anomaly from 1973-1983. Walsh and Johnson (1979) found that these long-term ice anomalies were negatively correlated with the 24-month running mean air temperature anomalies for the polar cap north of 60°N: specifically, the atmosphere was anomalously warm (cold) during periods of less (greater) than normal ice extent (see Fig. 6 in Walsh and Johnson, (1979)). A further examination of this correlation on a region-by-region basis will be presented in a future paper (see also Manak, 1988).

In section 3 it was hypothesized that the severe ice conditions in the Labrador Sea during winter 1983 were produced by atmospheric circulation anomalies associated with the 1982-83 ENSO event. Recently, it has been shown (e.g. Semazzi et al., 1988) that global sea surface temperature (SST) anomalies associated with ENSO events may also be related to the sub-Saharan rainfall anomalies, which have approximately decadal time scales (see Fig. 14). (It is important to note here that we are strictly referring to rainfall anomalies or fluctuations which are superimposed on long-term trends that may be due to land surface processes.) Thus it is natural to ask whether the Arctic sea ice anomalies bear any relationship with these rainfall anomalies. In this regard it is tantalizing to note that the severe drought conditions in both the Sabel and Soudan zones that prevailed in the early 1970's (with peaks in 1972 and 1973 respectively) coincided with the beginning of a sustained period of less than normal areal sea ice extent (cf. Figs. 13 and 14). The SST anomalies on a global scale may be the connecting link here, but unfortunately the SST data analyzed by Semazzi et al. stop at 60°N. It has been shown by Flemming (1987) that ice edge positions in the Labrador and Greenland Seas are quite closely related to the SST anomalies; thus a further study of ice, SST and rainfall data based on longer records may be warranted.

b) **The seven subregions**

Figures 15 to 21 show the smoothed monthly areal anomalies for regions 1 to 7, respectively. From the 25-month smoothed plots, we see that the anomalies are largest in regions 4, 5, and 6 (i.e. Baffin

Bay/Labrador Sea, Greenland Sea, and Barents & Kara Sea regions). The large positive anomaly in region 5 centered around 1968 is about 25% of the seasonal cycle and will be discussed further in §6. As would be expected, the anomaly magnitudes are smaller in those regions where ice variance is limited by land boundaries. Thus, for example, the anomalies in region 2 are only up to 15-20% of the seasonal cycle.

From Figs. 15-21 it is noted that the time scale of the smoothed anomaly fluctuations varies from region to region. The 25-month smoothed anomalies in regions 1 and 2 have an approximate 4-6 year cycle, whereas in region 6 (Barents & Kara Seas) there is a strong decadal cycle. There is also some evidence of a decadal cycle in regions 4 and 5. Regions 3 and 7 show more of a mixed signal.

Our identification of the interannual signal in regions 1 and 2 is consistent with the findings of Barnett (1980) who noted a 4-6 y fluctuation in the severity of ice conditions off the north coast of Alaska. It is also significant that in this general region fluctuations of various atmospheric and oceanic variables have similar time scales. For example, the spectrum of summer air temperature at Point Barrow, Alaska shows a well-defined 4-5 year peak (Rogers, 1977). A 5-6 year cycle has also been detected in the SST and sea level fluctuations in the Northeast Pacific (Mysak et al., 1982), which may also produce interannual fluctuations in some of the regional fish populations.

We offer two possible explanations for the 4-6 year cycle in the sea ice extent anomalies in the Bering Sea and western Arctic (regions 1 and 2). One might argue: that some of the negative ice anomalies are due to atmospheric circulation anomalies associated with the

mature phase of ENSO events, which take place every 2-7 years in the tropical Pacific (Mysak, 1986). Via the PNA teleconnection pattern (Fig. 8), a deep and intensified Aleutian low would transport considerable warm air during winter from the subtropics into the Bering and Chukchi Sea region. Thus, for example, less ice than normal would be expected during the winters of 1958, 1973 and 1983, which are the years corresponding to the mature phase of all the strong ENSO's since 1953 (Mysak, 1986, Table 1). However, examination of Figs. 15 and 16 reveals that during these years, there were low ice concentrations in regions 1 and 2 only in 1958. In some cases, just the opposite situation prevailed. For example, in region 2 during 1983 there was more ice than normal, probably due to the atmospheric conditions described in §3, which were not directly related to the PNA teleconnection pattern.

A more likely explanation for the 4-6 y cycle may be related to the natural interannual variability in the North Pacific sea level pressure (SLP), which may or may not be correlated with the ENSO events. Emery and Hamilton (1985) examined a series of seasonal mean SLP charts for the winters of 1947-1982. They found that the SLP patterns differed from climatology in one of the two following ways. Some winters had a strong circulation associated with an intensified Aleutian low (not necessarily related to ENSO), whereas other winters had weak atmospheric circulation due to the westward displacement of the Aleutian low and the presence of a weaker low off the west coast of the United States. Since 1953, this second type of anomalous circulation occurred in the winters of 1956, 1957, 1962, 1965, 1968, 1969, 1971, 1972, 1980 and 1982 (Emery and Hamilton, 1985, Table 1).

It is interesting to note that in six of these years (1956, 1957, 1965, 1971, 1972 and 1980) there was substantially more ice than normal in regions 1 and 2, and in two other years (1968 and 1969) the ice conditions were near normal (see Figs. 15 and 16). However, to further understand the processes associated with this air/ice relationship, more data need to be examined, including SLP from the Beaufort basin.

The origin of the approximately decadal sea ice fluctuations noted in regions 4, 5 and 6, which are contiguous with the North Atlantic Ocean, is not clear. However, there are at least three possible sources for this signal. First, it is now fairly well established that SST anomaly fluctuations in the North Atlantic tend to have decadal rather than interannual time scales (e.g., Semazzi et al., 1988; Wallace and Jiang, 1988, Fig. 23). Thus it might be anticipated that the ice edge position in the Labrador, Greenland and Barents Seas would vary in concert with these fluctuations: during anomalously warm (cold) ocean periods, the ice edge would be further north (south). A second cause of the decadal ice fluctuations may be the North Atlantic Oscillation (NAO) (e.g., Rogers, 1984), which is characterized by a fluctuation in the intensity of the westerly winds between the Icelandic low and the Azores high. However, the spectrum of the NAO shows a peak at about 4 y (R. Meyers, personal communication, 1988), which is closer to the period of the Southern Oscillation than the decadal time scale of interest here. A third and perhaps the most promising explanation for the decadal ice fluctuations is related to the fact that the "circuit time" for a water parcel in the North Atlantic subpolar gyre is about 10-15 y.

Thus any persistent ocean anomaly that is transported in this gyre and affects the ice concentration (e.g., the near-surface salinity) could result in decadal fluctuations in the ice extent provided such oceanic anomalies are generated or enhanced every decade or so. We shall return to this intriguing possibility in section 6.

We conclude this discussion of the regional anomalies by pointing out the well known out of phase behaviour between the sea ice anomalies in the Beaufort and Greenland Sea regions. That is, during heavier ice years in the Greenland Sea there is lighter than normal ice coverage in the Beaufort Sea region, and vice-versa. This pattern is clearly evident in Figure 22 which shows the superposition of the 25-month running means of the anomalies in these two regions. During the 32 year period 1953-84, the anomalies centered around 1956, 1961, 1968, 1975, 1979, and 1983 are out of phase.

The results shown in Fig. 22 are consistent with the findings of Walsh and Johnson (1979), who used EOF's of longitude to identify the major spatial scales of ice fluctuations during 1953-77. They found the North Atlantic anomalies to be out of phase with the anomalies over the rest of the polar cap. Smirnov (1980) also noted the out of phase relationship between ice anomalies in the western and eastern parts of the non-Soviet Arctic. He found that the ice anomalies were of opposite sign in 82% of the cases. A short time shift was also noted between the anomalies in the eastern and western regions, with the east leading by one to two months. That is, ice extent in the Greenland Sea in July can be used to estimate ice extent in the Beaufort Sea in August. Smirnov attributed the opposition between the western and eastern regions to atmospheric processes in the northern

parts of the central and eastern regions. We argue here that this out of phase ice anomaly behaviour is most likely caused by very large scale atmospheric circulation anomalies which also produce the seesaw in winter air temperatures between Greenland and northern Europe (van Loon and Rogers, 1978).

It has been known for some time (see van Loon and Rogers, 1978, and the references therein) that when winter temperatures are low over northern Europe (e.g., in Oslo), they tend to be high over western Greenland (e.g., Jakobshavn) and the Canadian Arctic, and vice versa. Van Loon and Rogers found that well-defined SLP anomalies, over most of the Northern Hemisphere, are associated with the above temperature seesaw and are distributed as follows: During the GB case (Greenland temperature below the mean, Oslo temperature above the mean), the SLP in January generally exhibits an anomalously deep and intensified Icelandic low over the North Atlantic and an anomalously weak Aleutian low over the North Pacific. Thus with reference to the North Atlantic more cold air than usual would be advected southward into the Greenland Sea and Baffin Bay region, making Jakobshavn very cold and producing more ice in regions 4 and 5. At the same time, a weaker than normal Aleutian low would presumably pull down less cold polar air into the Beaufort & Chukchi Seas (region 2) and hence give less severe ice conditions there, in contrast to the situation in region 5. Rogers and van Loon (1979) showed that during the GB case ice conditions in Davis Strait (in the central part of region 4) remain severe throughout spring and summer and that icebergs are more frequent in spring off of Newfoundland, which is consistent with the first part of our argument. However, they did not make any

association of the SLP anomalies with the ice conditions in region 2. Finally, we note that during the GA case (Greenland temperature above normal, Oslo temperature below normal), the SLP anomalies over the North Atlantic and North Pacific are reversed, which would tend to produce less ice than usual in regions 4 and 5 and more ice in region 2. Since the results presented by van Loon and Rogers were mostly in the form of correlations, it is not possible to examine the actual year-to-year variations in the SLP anomalies and hence compare these with the time series of ice anomalies as shown in Fig. 22.

6. The Greenland Sea ice anomaly of 1963-72

One of the most remarkable anomalies seen in all of the sea ice maps published by Manak and Mysak (1987) is the extended position of the Greenland Sea ice edge during 1963-72, which also shows up as a broad peak in the 25-month smoothed anomaly curve in Fig. 19. Figure 23 shows the bi-yearly sequence of winter maps of sea ice extent for the latter part of this period, along with the 9/10 contour of winter climatology taken from Fig. 5. From these maps, we can see that a large Greenland Sea ice anomaly was well established in winter of 1966, achieved a maximum in 1968, was present along the whole east coast of Greenland in 1970 and persisted well into the winter of 1972. The amplitude of this anomaly is even more impressive when one recalls the relatively small size of the seasonal cycle in the Greenland Sea (Fig. 12). We also note in Fig. 23 the appearance of a large positive ice anomaly in the Labrador Sea in 1972 (see also Fig. 18 which shows that this anomaly lasted from 1970 to 1974). In view of the magnitude and time evolution of these anomalies, it is natural to hypothesize that the Labrador Sea anomaly may be related to the Greenland Sea anomaly. Alternatively, as a second hypothesis one might suppose that the Labrador Sea anomaly is simply due to anomalous local atmospheric and oceanic conditions. Figure 24 (top panel) shows that during winter of 1972 there was a deep and intensified Icelandic low centered near the southern tip of Greenland. The surface winds associated with this low would have advected southward cold air and ice from the Baffin Bay region into the Labrador Sea and hence produced heavier ice conditions there. At the same time, there were significant cold SST anomalies in the Labrador Sea (Fig. 24, lower panel) which also would

have contributed to the greater extent of sea ice. From these data, one might thus readily accept the second hypothesis regarding the local generation of the 1972 Labrador Sea ice anomaly. However, a comparison of the smoothed anomalies in Figs. 18 and 19, together with a study of the regional ocean circulation pattern (Fig. 4) strongly suggests that there could be considerable merit in the first hypothesis.

Figure 25 shows the superposition of the 25-month smoothed anomaly time series for regions 4 and 5. This figure reveals that during 1953-84 both positive and negatively ice anomalies in the Greenland Sea tend to lead similar anomalies in the Labrador Sea by 3-4 years. In particular, the peaks in the Labrador Sea ice anomaly curve centered around 1958, 1967 and 1972 follow peaks in the Greenland Sea curve centered around 1954-55, 1963 and 1968. Since the distance from the northwest part of the Greenland Sea to the central part of the Labrador Sea is about 4000 km, this yields a speed of anomaly "propagation" of about 1000 km/y or 2.7 km/d (3.2 cm/s). It is significant to note that this speed of ice anomaly movement is roughly the same as the average current speed of the North Atlantic subpolar gyral circulation, viz., 2-3 cm/s (Parkinson et al., 1987). Thus this gyre, which circulates cyclonically in the northern North Atlantic Ocean, and the Norwegian, Greenland and Labrador Seas could account for the apparent movement of the ice anomalies from the Greenland Sea into the Labrador Sea if there were some water mass anomalies being advected by the currents that strongly affect ice concentration or ice formation. We propose here that salinity anomalies are the connecting link. For example, in relatively fresh

waters more ice will tend to form due to the higher freezing point. In particular, if the salinity in the Greenland Sea is less than the critical value of 34.7, the cooler, fresher surface layer will not reach a high enough density, even at the freezing point, to mix with the warmer, more saline water underneath, and ice will tend to form (Dickson et al., 1975).

What lends credence to the first hypothesis is that the movement of the "1968" Greenland Sea ice anomaly into the Labrador Sea coincided with the advection of a mass of anomalously low salinity water (the "Great Salinity Anomaly") around the subpolar gyre in the northern North Atlantic (Dickson et al., 1988). This salinity anomaly, which extended to a depth of 500-800 m, was first observed north of Iceland in the 1960's (reaching a minimum of about 34.2 in 1968 - see Fig. 2 in Dickson et al., 1975), was next found in the Labrador Sea during 1971-72 (Lazier, 1980, Fig. 2; see also Ikeda, 1987, and Lazier, 1988) and was then subsequently traced around the subpolar gyre until it returned to the Greenland Sea in 1981-82. The advection speed of the Great Salinity Anomaly is estimated to be about 3 cm/s (Dickson et al., 1988) which compares very favourably with our estimate of 3.2 cm/s for the propagation speed of the ice anomalies. Therefore, it is quite conceivable that the two anomalies could be related (see also Manak, 1988, for a further discussion).

It has been suggested by Dickson et al. (1975) that the Great Salinity Anomaly in the Greenland Sea was indirectly due to an anomalous atmospheric circulation pattern over Greenland. Dickson et al. have documented the existence of an anomalously high pressure cell during winter over Greenland between the early 1950's and the late

1960's. The development and evolution of this high can also be seen in the winter SLP maps in Allingham et al. (1987). These maps show a strong high over Greenland during 1959-62, a fairly weak circulation there from 1963-65, and then again an intense anticyclonic circulation during 1966-69. From 1970 onward for several years, the winter atmospheric circulation was near normal.

The persisting and amplifying anticyclone over Greenland during 1959-62 strengthened the northerlies in the Greenland Sea, resulting in lower mean winter air temperatures (Dickson et al., 1975). Also, the anomalous winds resulted in more fresh water and probably more ice being transported south in the East Greenland Current towards Iceland during the early 1960's. The effect of this atmospheric circulation anomaly on the areal sea ice extent in region 5 is indeed dramatic: from 1959-62 there was a large increase in the smoothed ice anomaly (Fig. 25). Similarly, the patterns of weak, strong and normal atmospheric circulation after this coincided respectively with the constant positive ice anomaly from 1963-66, the large peak from 1967-70 and the nearly zero anomaly conditions after 1971.

7. Summary and concluding remarks

The seasonal and interannual variability of sea ice extent in the Arctic has been investigated for the 32-y period 1953-84. The major findings of our study are summarized below:

1) The climatological ice edge positions in the various subregions of the Arctic are largely determined by the surface ocean circulation patterns at high latitudes and mark the northern boundary of the highly biologically productive "Marine Subarctic" region.

2) The time scale of the areal sea ice anomaly fluctuations varies from region to region: a) In the western Arctic (regions 1 and 2), the smoothed anomalies exhibited an approximate 4-6 y cycle, most likely due to the interannual variability of the sea level pressure in the North Pacific and the Beaufort & Chukchi Sea region. b) There is a strong decadal cycle in the smoothed anomalies for the Barents & Kara Seas (region 6); this fluctuation is also partially evident in regions 4 and 5. It is speculated that this time scale is set by the "circuit time" of the subarctic gyre in the northern North Atlantic. c) In intermediate regions 3 and 7, the time scale of the anomaly fluctuations appears to vary from interannual to decadal.

3) An out of phase relationship was noted between the 25-month smoothed anomalies in the Beaufort & Chukchi Sea region and the Greenland Sea, in agreement with some earlier studies. It is proposed that this behaviour is related to atmospheric pressure

anomalies associated with the seesaw in winter air temperature between northern Europe and western Greenland.

4) A particularly significant positive ice anomaly was detected in the Greenland Sea for the 1963-72 period; its maximum occurred in 1968 and was 35% of the seasonal signal. A large positive anomaly was also seen in the Labrador Sea during 1970-74, with its maximum occurring in 1972. It appears that the latter anomaly originated in the Greenland Sea, and persisted due to the presence of a large negative salinity anomaly which moved cyclonically around the subarctic gyre with a speed of about 3 cm/s. Thus the ice anomaly was seen to "propagate" down the east coast of Greenland and up its west coast in conjunction with the movement of the salinity anomaly.

The results described in summary item 4) above may be important for long-range climate prediction. A salinity or ice anomaly off of Greenland can be used to predict anomalies in ice extent in the Labrador Sea 3-4 years later. Also, since air temperature and sea ice extent are negatively correlated (Walsh and Johnson, 1979; Manak, 1988), anomalous ice conditions in the Greenland Sea can be used to predict anomalous air temperatures in the Labrador Sea region 3-4 years in advance. To test this potential application of our findings, further study of historical records of the ice edge position in the Greenland and Labrador Seas is recommended. One particularly useful data source may be the ice charts produced by the Danish Meteorological Institute. From these data, Kelly (1979) has produced a digital-format circumpolar ice limit for the years 1901-56. The data are

conveniently displayed on the one-degree grid shown in Fig. 1, and thus could also be used to verify the time scales of the anomaly fluctuations summarized in item 2) above, and to explore further the out of phase relation between the anomalies in the western and eastern Arctic regions (item 3) above).

Acknowledgements

It is a pleasure to thank J.E. Walsh for the ice concentration data and helpful discussions, A. Cossette for typing the manuscript and U. Seidenfuss for preparing some of the figures. This work was supported by NSERC (in the form of an Operating Grant to L.A.M. and a Postgraduate Scholarship to D.K.M.), FCAR and the U.S. Office of Naval Research, Code 1122 PO. During the course of this work, L.A.M. was also supported by an AES/NSERC Industrial Research Chair in Climatology.

References

Allingham, A.M., K. Hamilton and L.A. Mysak. 1987. Climatic Atlas of the North Atlantic - Seasonal Sea Level Pressures and Sea Surface Temperature Anomalies, 1919-1979. Climate Research Group Report 87-4, Dept. of Meteorology, McGill University, Montreal, Que., 248 p.

Barnett, D.G. 1980. A long-range ice forecasting method for the north coast of Alaska. In Proceedings of the Arctic Ice Dynamics Joint Experiment international commission on snow and ice symposium, (ed. R.S. Pritchard), 360-372, University of Washington Press, Seattle.

Dickson, R.R., H.H. Lamb, S.A. Malmberg and J.M. Colebrook. 1975. Climatic reversal in the northern North Atlantic. Nature, Lond., 256: 479-482.

Dickson, R.R., J. Meincke, S. Malmberg and A.J. Lee. 1988. The "Great Salinity Anomaly" in the northern North Atlantic, 1968-82. Prog. in Oceanogr., (in press).

Dunbar, M.J. 1986. Arctic marine ecosystems. Oceanus, 29: 36-40.

Emery, W.J. and K. Hamilton. 1985. Atmospheric forcing of interannual variability in the northeast Pacific Ocean: connections with El Niño. J. Geophys. Res., 90: 857-868.

Flemming, G.H. 1987. Predictability of Ice Concentration in the High-latitude North Atlantic from Statistical Analysis of SST and Ice

Concentration Data. M.Sc. thesis, Naval Postgraduate School, Monterey, CA.

Hibler III, W.D. and K. Bryan. 1987. A diagnostic ice-ocean model. J. Phys. Oceanogr., 17: 987-1015.

Ikeda, M. 1987. Salt and heat balances in the Labrador Sea using a box model. Atmos.-Ocean, 25: 197-223.

Kelly, P.M. 1979. An Arctic sea ice data set, 1901-1956 World Data Center-A for Glaciology (Snow and Ice), Boulder, CO., Glaciological Data Report GD-5, pp 101-106.

Lazier, J.R.N. 1980. Oceanographic conditions at Ocean Weather Ship BRAVO 1964-1974. Atmos.-Ocean, 18: 227-238.

Lazier, J.R.N. 1988. Temperature and salinity changes in the deep Labrador Sea; 1962-1986. Deep-Sea Res., (in press).

Lemke, P., E.W. Trinkl and K. Hasselmann. 1980. Stochastic dynamic analysis of polar sea ice variability. J. Phys. Oceanogr., 10: 2100-2120.

Manak, D.K. 1988. Climatic Study of Arctic Sea Ice Extent and Anomalies 1953-1984. M.Sc. thesis, McGill University, Montreal, Que., 67 p.

Manak, D.K. and L.A. Mysak. 1987. Climatic Atlas of Arctic Sea Ice Extent

and Anomalies, 1953-1984. Climate Research Group Report 87-8, Dept. of Meteorology, McGill University, Montreal, Que., 214 p.

McLaren, A.S., M.C. Serreze and R.G. Barry. 1988. Seasonal variations of atmospheric circulation and sea ice motion in the Arctic. Extended abstract from Preprints, Second Conference on Polar Meteorology and Oceanography, 20-23, Amer. Meteorol. Soc., Boston, Mass.

Mysak, L.A. 1986. El Niño, interannual variability and fisheries in the northeast Pacific Ocean. Can. J. Fish. Aquat. Sci., 43, 464-497.

Mysak, L.A., W.W. Hsieh and T.R. Parsons. 1982. On the relationship between interannual baroclinic waves and fish populations in the Northeast Pacific. Biol. Oceanogr., 2: 63-103.

Nicholson, S.E. 1985. Sub-Saharan rainfall 1981-84. J. Clim. Appl. Meteorol., 24: 1388-1391.

Parkinson, C.L. and D.J. Cavalieri. 1988. Arctic sea ice 1973-1986: seasonal and interannual variability. Extended abstract from Preprints, Second Conference on Polar Meteorology and Oceanography, 4-7, Amer. Meteorol. Soc., Boston, Mass.

Parkinson, C.L., C.C. Josefino, H.J. Zwally, D.J. Cavalier, P. Gloersen and W.J. Campbell. 1987. Arctic Sea Ice 1973-1976: Satellite Passive Microwave Oservations, NASA SP-489, National Aeronautics and Space Administration, Washington, D.C., 296 p.

Rasmusson, E.M. and J.M. Wallace. 1983. Meteorological aspects of the El Niño/Southern Oscillation. Science (Wash., D.C.), 222: 1195-1202.

Rogers, J.C. 1977. A meteorological basis for long-range forecasting of summer and early autumn sea ice conditions in the Beaufort Sea. In Proceedings of Fourth International Conference on Port and Ocean Engineering under Arctic Conditions, 2, (ed. D.B. Muggeridge), pp. 952-962, Memorial University of Newfoundland, St. John's, Nfld.

Rogers, J.C. 1984. The association between the North Atlantic Oscillation and the Southern Oscillation in the Northern Hemisphere. Mon. Wea. Rev., 112: 1999-2105.

Rogers, J.C. and H. van Loon. 1979. The seesaw in winter temperatures between Greenland and northern Europe. Part II: Some oceanic and atmospheric effects in middle and high latitudes. Mon. Wea. Rev., 107: 509-519.

Ross, B. and J.E. Walsh. 1988. Long-range forecasts of Arctic sea level pressure. Extended abstract from Preprints, Second Conference on Polar Meteorology and Oceanography, 48-51, Amer. Meteorol. Soc., Boston, Mass.

Semazzi, F.H.M., V. Mehta and Y.C. Sud. 1988. An investigation of the relationship between sub-Saharan rainfall and global sea surface temperatures. Atmos.-Ocean, 26: 118-138.

Semtner, A.J. Jr. 1987. A numerical study of sea ice and ocean circulation in the Arctic. J. Phys. Oceanogr., 17: 1077-1099.

Smirnov, V.I. 1980. Opposition in ice redistribution in the waters of the foreign Arctic. Meteorol. Gidrol., No. 3: 73-77.

Untersteiner, N. (editor) 1986. The Geophysics of Sea Ice. NATO ASI Series B: Physics Vol. 146. Plenum Press, New York, 1196 p.

van Loon, H. and J.C. Rogers. 1978. The seesaw in winter temperatures between Greenland and northern Europe. Part I: General description. Mon. Wea. Rev., 106: 296-310.

Wallace, J.M. and Q. Jiang. 1988. Large-scale atmosphere/ocean interaction in northern winter. Mon. Wea. Rev., submitted.

Walsh, J.E. 1983. The role of sea ice in climatic variability: Theories and evidence. Atmos.-Ocean., 21: 229-242.

Walsh, J.E. and C.M. Johnson. 1979. An analysis of Arctic sea ice fluctuations. J. Phys. Oceanogr., 9: 580-591.

Willmott, A.J. and L.A. Mysak. 1988. A simple steady-state coupled ice-ocean model, with application to the Greenland-Norwegian Sea. J. Phys. Oceanogr., submitted.

Zwally, H.J., J.C. Comiso, C.L. Parkinson, W.J. Campbell, F.D. Carsey and P. Gloersen. 1983. Antarctic Sea Ice, 1973-1976: Satellite Passive-Microwave Observations. NASA SP-459 National Aeronautics and Space Administration, Washington, D.C., 206 pp.

TABLE 1

ICE DATA SOURCES

U.S. Navy/NOAA Joint Ice Center, Arctic Sea Ice Analyses (Eastern and Western), 1972-1984.

U.S. Naval Oceanographic Office, Report of the Arctic Ice Observing and Forecasting Program, 1953-1971.

Canadian Department of Transport, Annual Reports, 1964-1969.

British Meteorological Office, Monthly Ice Charts, 1959-1977.

Danish Meteorological Institute, The Ice Conditions of the Greenland Waters, 1957-1964.

Danish Meteorological Institute, The state of the ice in the Arctic Seas, 1953-1956.

Jokull (Icelandic journal), Annual ice summaries, 1953-1967.

Arbok Norsk Polarinstitut (Norwegian yearbook), 1963-1971.

Note: All grids for 1972-1984 are from the Navy/NOAA Joint Ice Centre's digital grids, transformed to the grid of Fig. 1.

TABLE 2

Names of subregions shown in Fig. 1

Region 1 - Bering Sea

Region 2 - Beaufort & Chukchi Seas

Region 3 - Hudson Bay

Region 4 - Baffin Bay, Davis Strait, Labrador Sea

Region 5 - Greenland Sea

Region 6 - Barents & Kara Seas

Region 7 - East Siberian & Laptev Seas

Figure captions

Fig. 1 The sea ice concentration grid (after Walsh and Johnson, 1979) and the seven subregions used in this study.

Fig. 2 Annual climatology of sea ice extent in the Arctic for the period 1953-84. The ice concentration contours are labelled in tenths (1 = 1/10 etc.).

Fig. 3 The Arctic basin showing the biologically productive "Marine Subarctic" region as shaded (from Dunbar, 1986). Also shown are the 1/10 and 5/10 ice concentration contours taken from Fig. 2.

Fig. 4 Schematic of the large-scale horizontal circulation patterns in the surface waters of the north polar region. (From Parkinson et al., 1987.)

Fig. 5 Seasonal climatologies of sea ice extent in the Arctic for the period 1953-84.

Fig. 6 Sea ice extent in the Arctic for autumn 1982 (top panel) and autumn 1983 (bottom panel).

Fig. 7 Yearly sequence of winter maps of sea ice extent from 1981-84.

Fig. 8 During the mature phase of a typical occurrence of the El Niño-Southern Oscillation phenomenon (December through February following the warming of South American coastal waters),

atmospheric anomalies at jet stream level (about 10 km) above the Pacific include a pair of anticyclones to the north and south of the equator associated with the eastward extension of cloud cover and rainfall (stippled areas). A triplet of anomalies occurs over the North Pacific, Canada, and the southern United States-western Atlantic (left). During the 1982-83 occurrence, however, the equatorial rainfall and anticyclonic anomalies migrated much farther east and the triplet of anomalies in the middle latitudes were much more intensified (right). (After Rasmusson and Wallace, 1983.)

Fig. 9 The normal seasonal cycle of areal sea ice extent in the Arctic.

Fig. 10 Seasonal cycles of areal sea ice extent in the Bering Sea (region 1) and the Beaufort & Chukchi Seas (region 2).

Fig. 11 Seasonal cycles of areal sea ice extent in Hudson Bay (region 3) and the Baffin Bay/Labrador Sea (region 4).

Fig. 12 Seasonal cycles of areal sea ice extent in the Greenland Sea (region 5), the Barents & Kara Seas (region 6) and the East Siberian & Laptev Seas (region 7).

Fig. 13 Smoothed time series of monthly anomalies of areal sea ice extent in the Arctic region. Light and dark curves correspond to 3-month and 25-month running means respectively.

Fig. 14 (a) Station network and location of rainfall zones.

(b) Standardized annual rainfall index for the Sahel and Soudan zones of sub-Saharan Africa. (From Nicholson, 1985.)

Fig. 15 Same as Fig. 13 except for Bering Sea.

Fig. 16 Same as Fig. 13 except for Beaufort & Chukchi Seas.

Fig. 17 Same as Fig. 13 except for Hudson Bay.

Fig. 18 Same as Fig. 13 except for Baffin Bay/Labrador Sea.

Fig. 19 Same as Fig. 13 except for Greenland Sea.

Fig. 20 Same as Fig. 13 except for Barents & Kara Seas.

Fig. 21 Same as Fig. 13 except for East Siberian & Laptev Seas.

Fig. 22 Superposition of the 25-month smoothed anomalies of areal sea ice extent in the Beaufort (region 2) and Greenland (region 5) Seas.

Fig. 23 Bi-yearly sequence of winter maps of sea ice extent from 1966 to 1972. The dashed line (e.g., in the Barents and Greenland Seas) corresponds to the 9/10 contour on the winter climatology map (see Fig. 5).

Fig. 24 Maps of North Atlantic sea level pressure (top, in mb) and sea surface temperature anomaly (SSTA) (bottom, in $^{\circ}C$) for winter (DJF) 1972. The SST anomalies represent the deviations of temperature from a 1946-79 climatology. (From Allingham et al., 1987.)

Fig. 25 Superposition of the 25-month smoothed anomalies of areal sea ice extent in the Greenland (region 5) and Labrador (region 4) Seas.

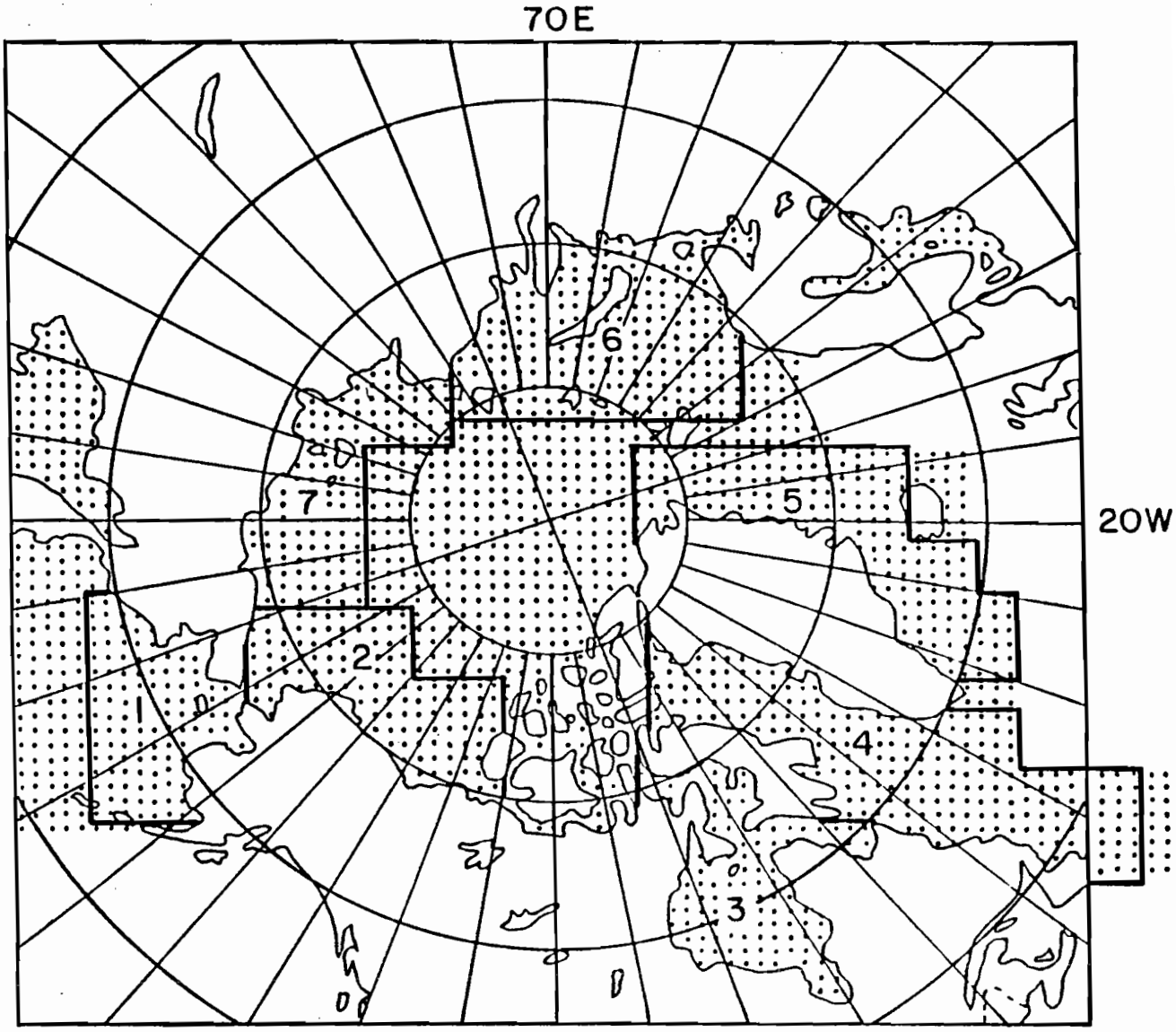

Fig. 1. The sea ice concentration grid (after Walsh and Johnson, 1979) and the seven subregions used in this study.

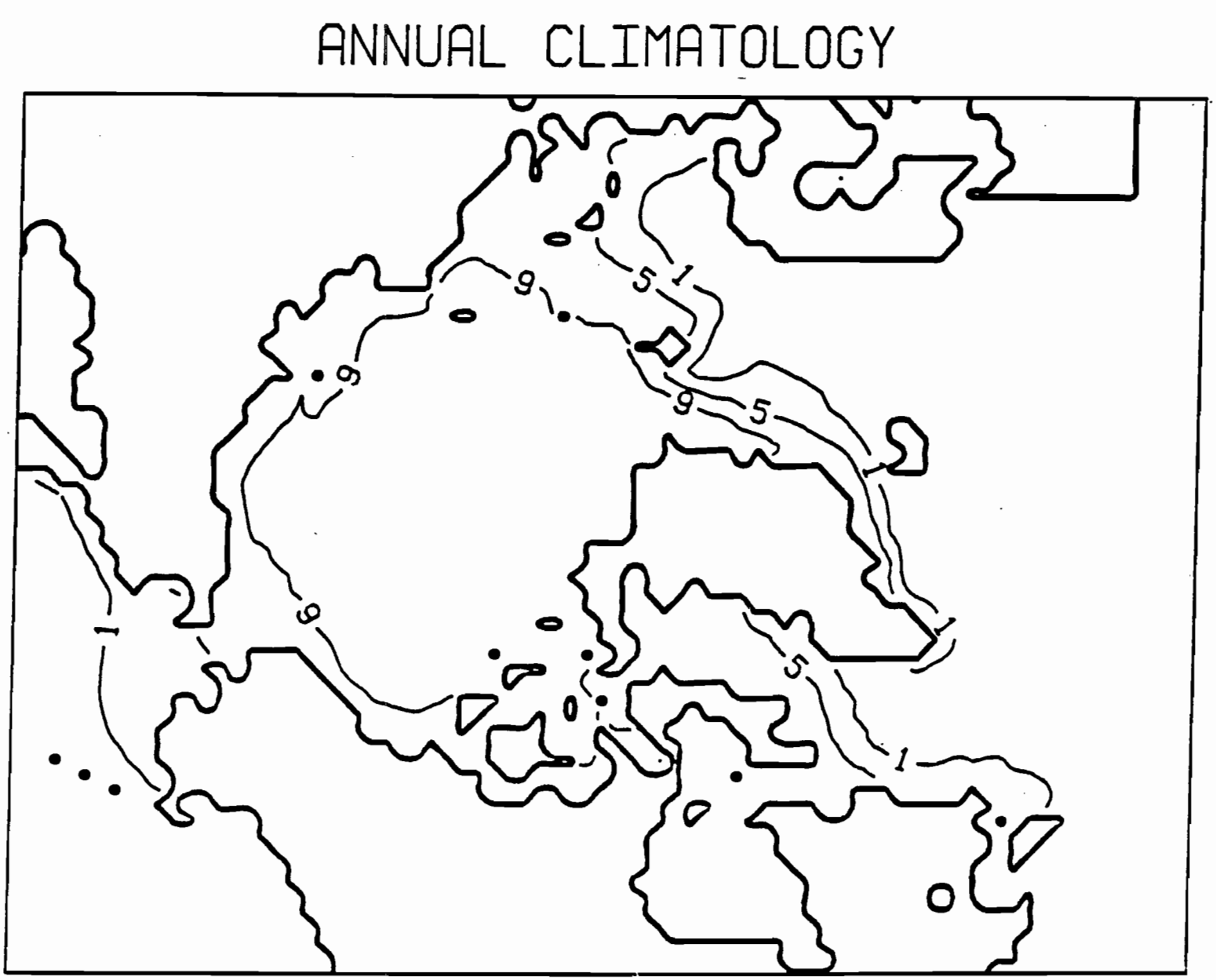

Fig. 2. Annual climatology of sea ice extent in the Arctic for the period 1953-84. The ice concentration contours are labelled in tenths (1 = 1/10 etc.).

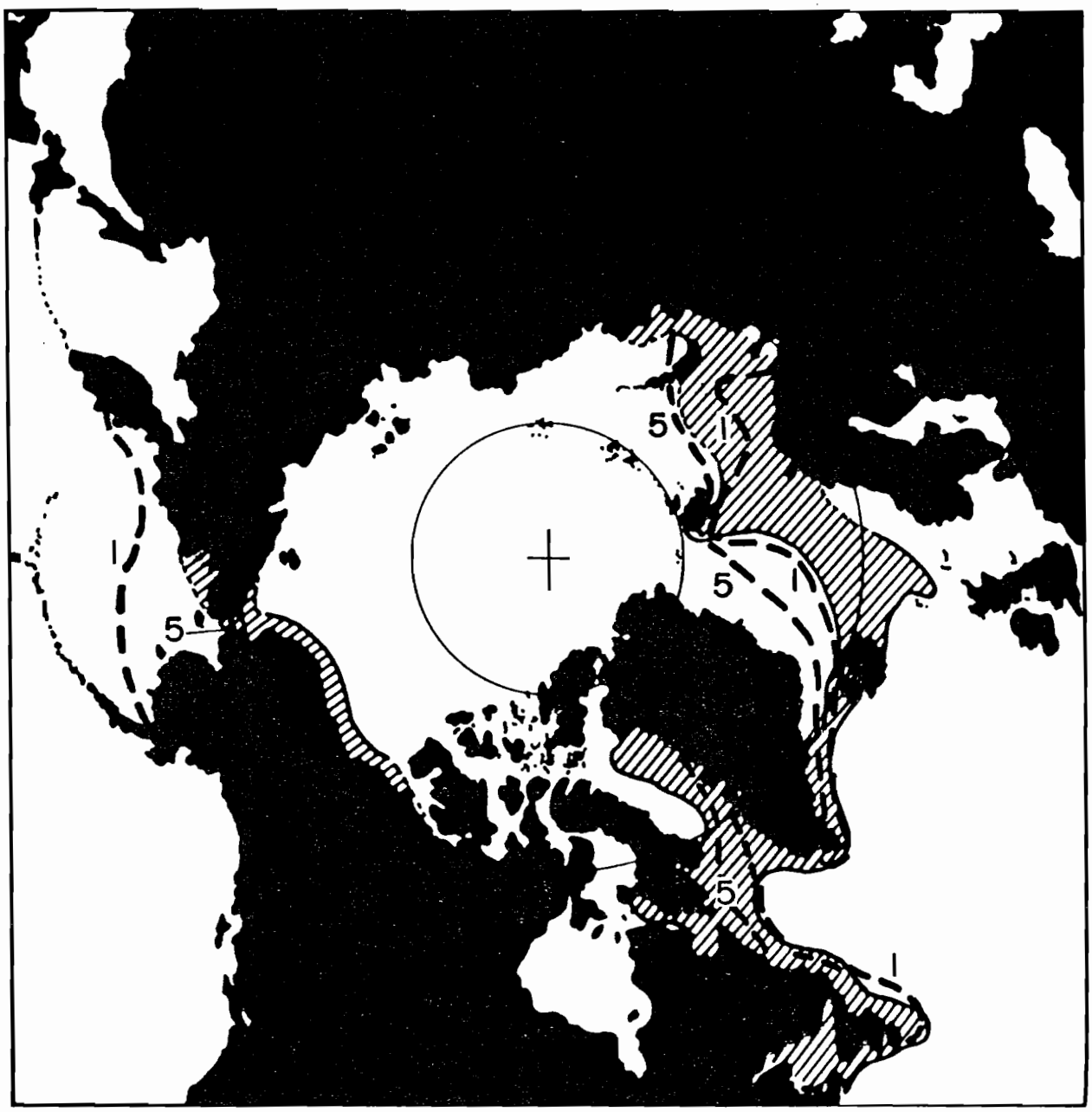

Fig. 3. The Arctic basin showing the biologically productive "Marine Sub-arctic" region as shaded (from Dunbar, 1986). Also shown are the 1/10 and 5/10 ice concentration contours taken from Fig. 2.

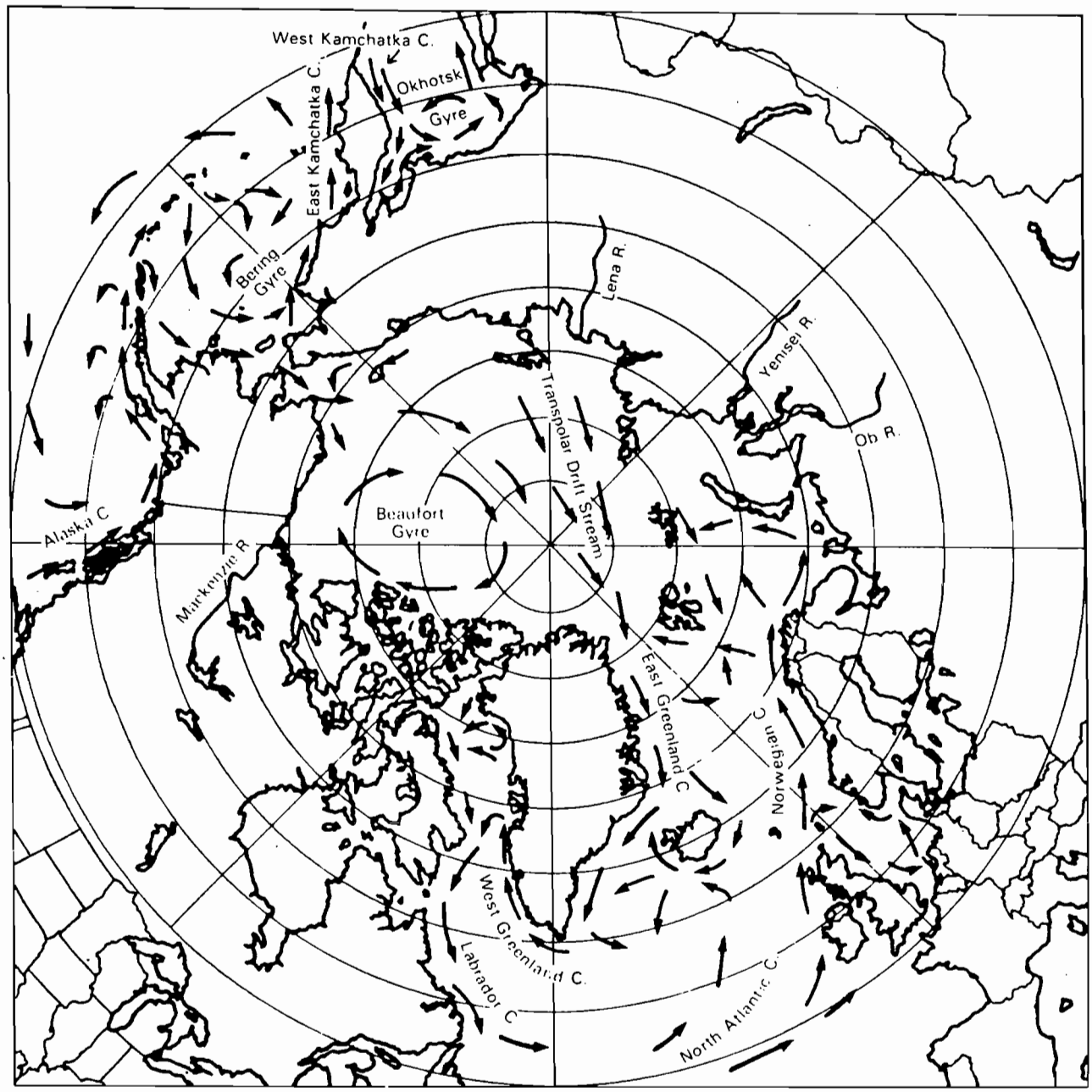

Fig. 4. Schematic of the large-scale horizontal circulation patterns in the surface waters of the north polar region. (From Parkinson et al., 1987.)

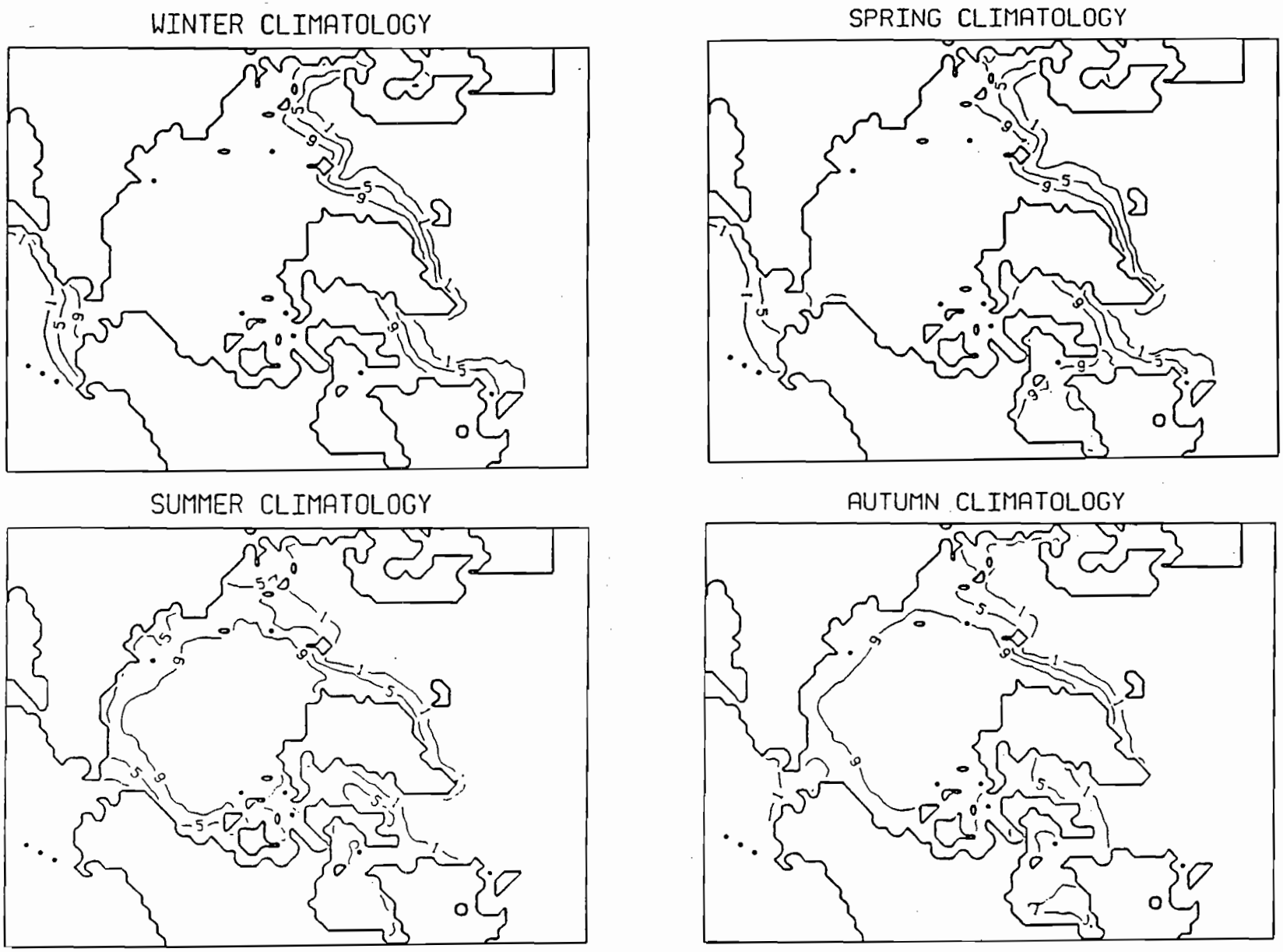

Fig. 5. Seasonal climatologies of sea ice extent in the Arctic for the period 1953-84.

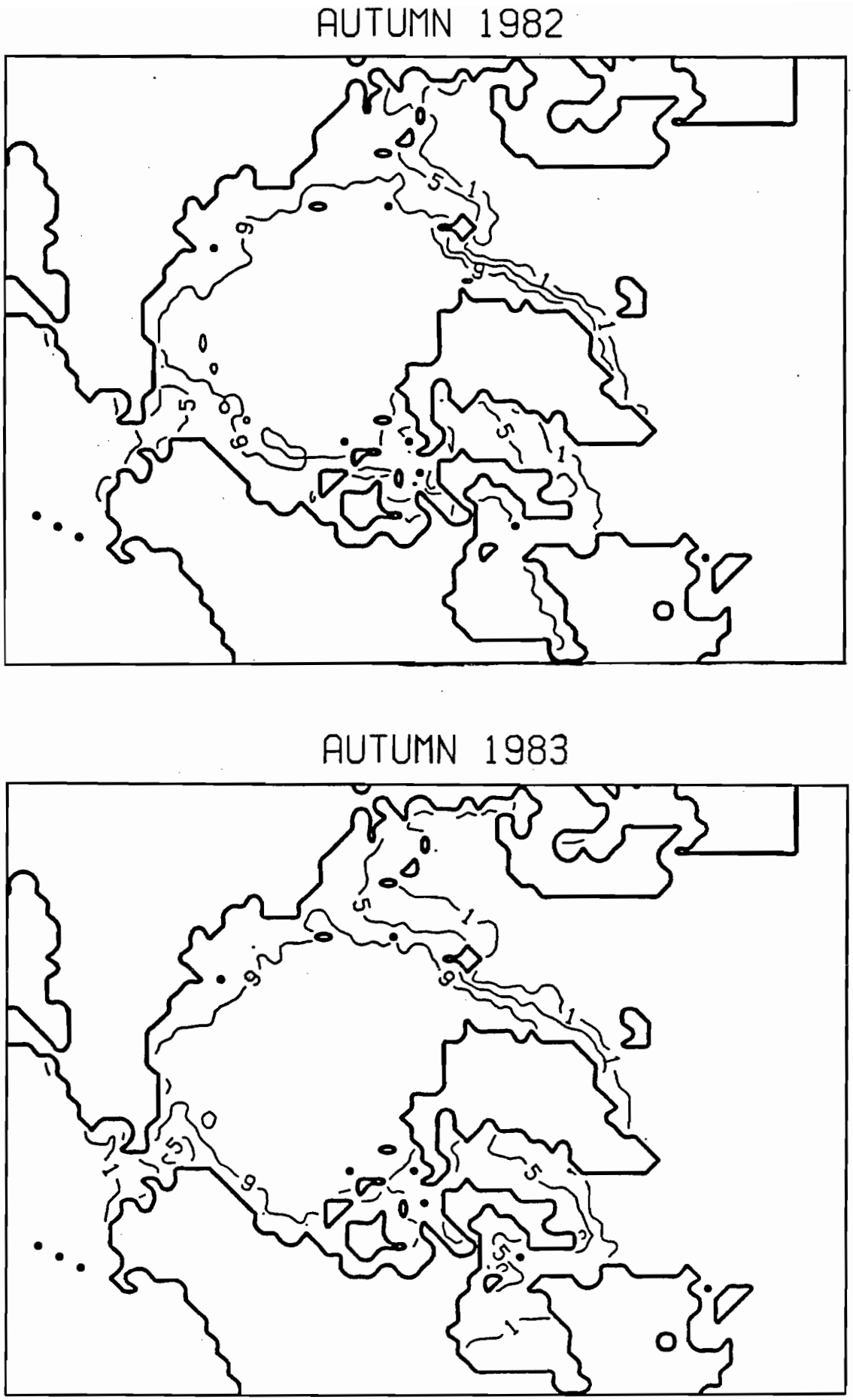

Fig. 6. Sea ice extent in the Arctic for autumn 1982 (top panel) and autumn 1983 (bottom panel).

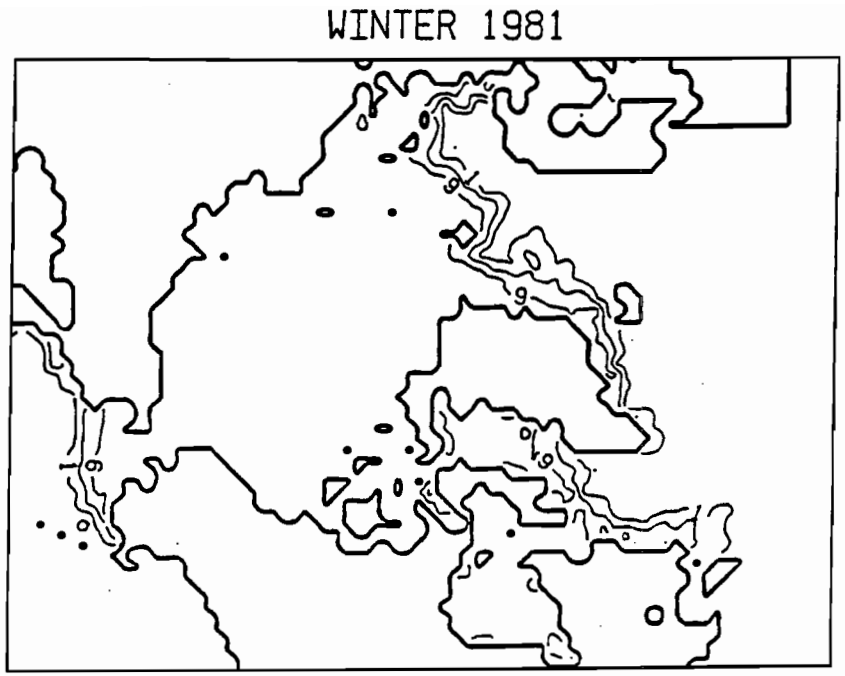

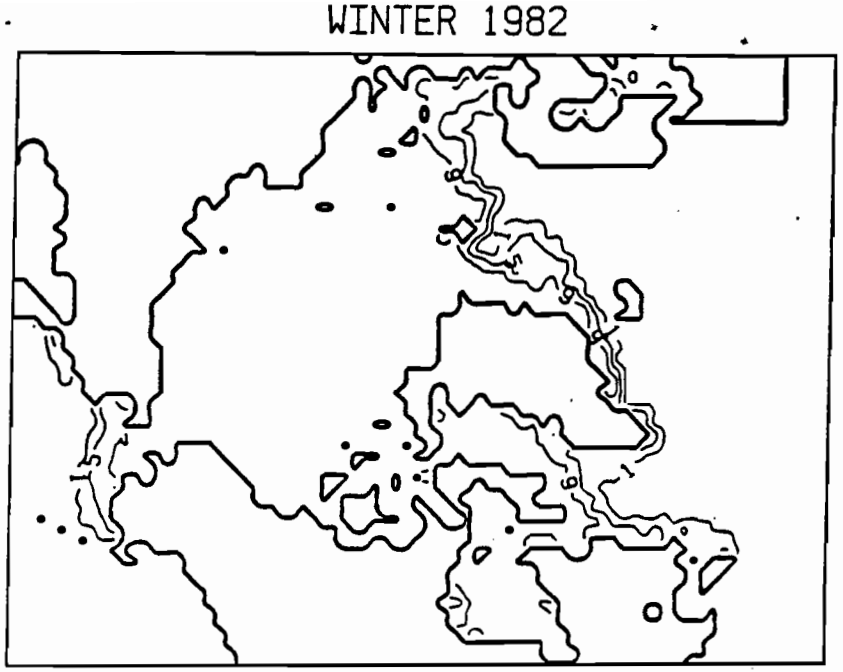

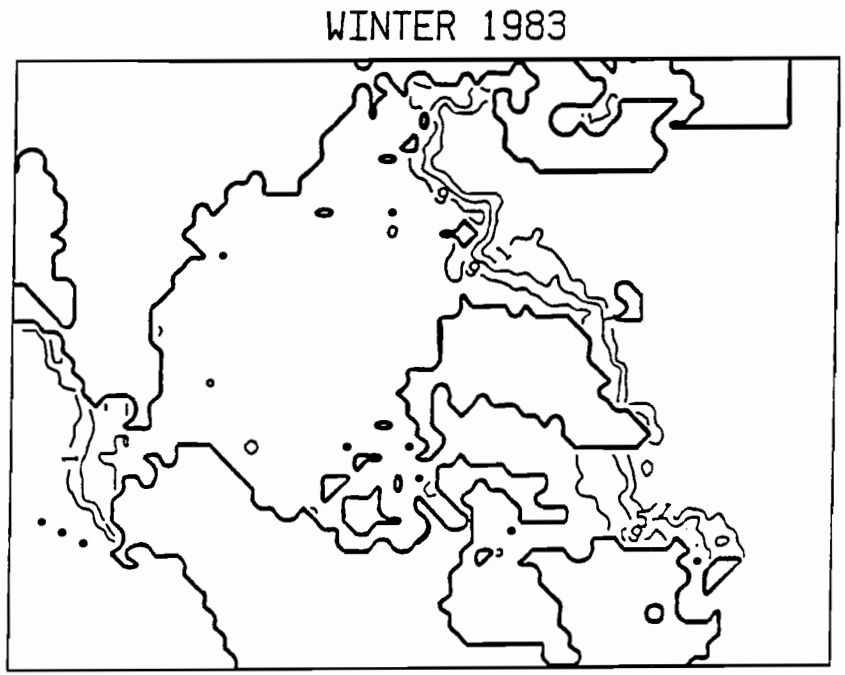

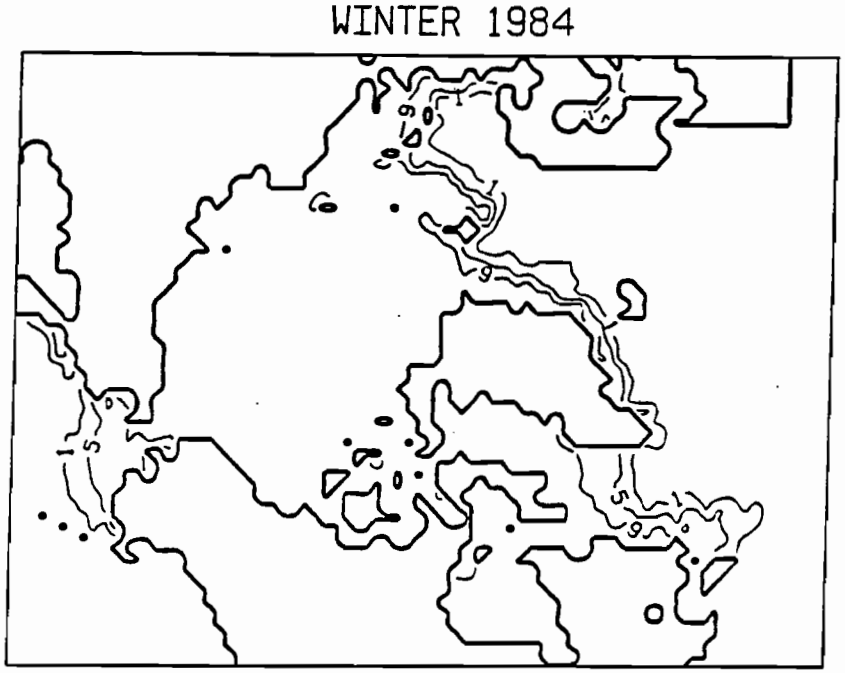

Fig. 7. Yearly sequence of winter maps of sea ice extent from 1981-84.

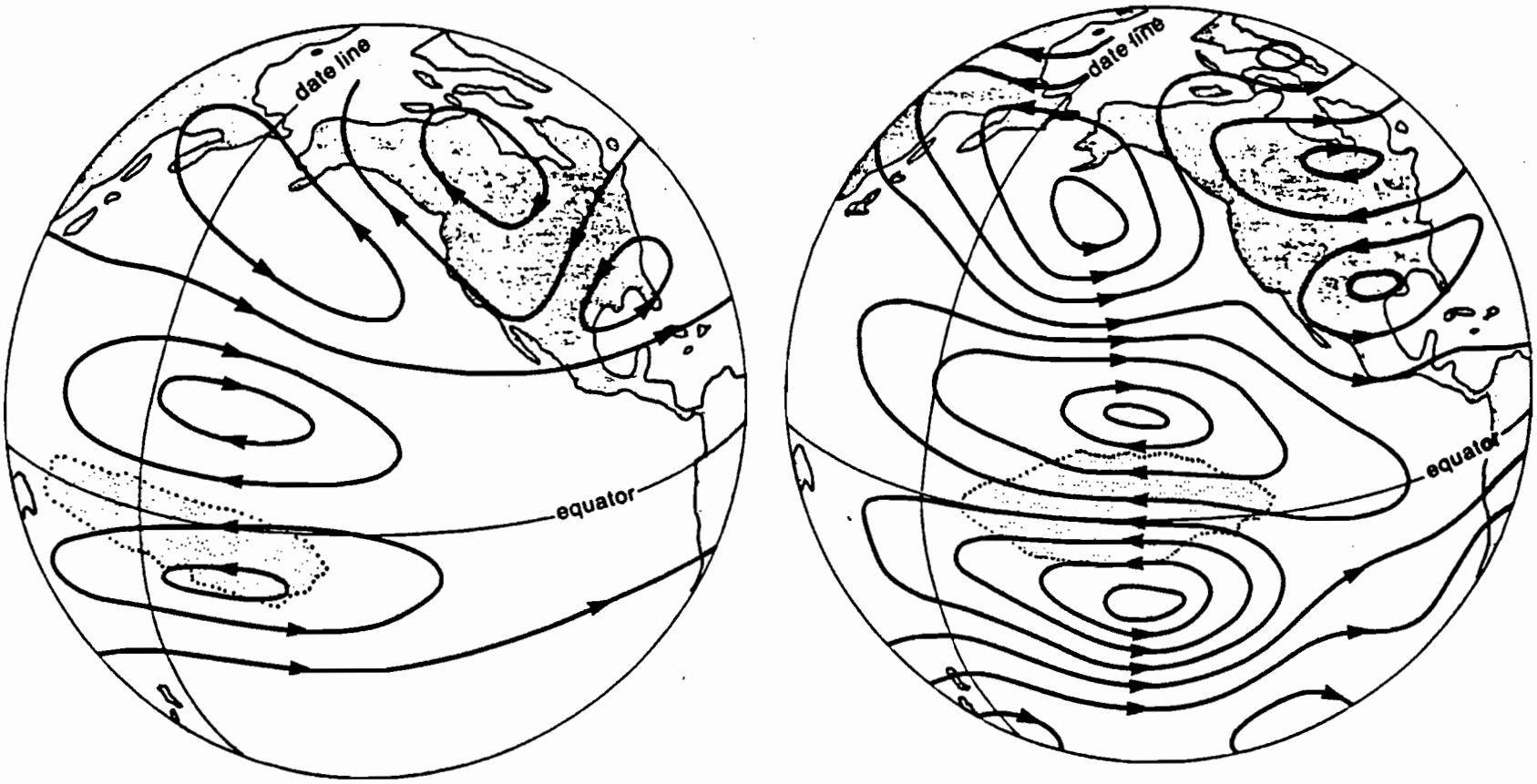

Fig. 8. During the mature phase of a typical occurrence of the El Nino-Southern Oscillation phenomenon (December through February following the warming of South American coastal waters), atmospheric anomalies at jet stream level (about 10 km) above the Pacific include a pair of anticyclones to the north and south of the equator associated with the eastward extension of cloud cover and rainfall (stippled areas). A triplet of anomalies occurs over the North Pacific, Canada, and the southern United States-western Atlantic (left). During the 1982-83 occurrence, however, the equatorial rainfall and anticyclonic anomalies migrated much farther east and the triplet of anomalies in the middle latitudes were much more intensified (right). (After Rasmusson and Wallace, 1983.)

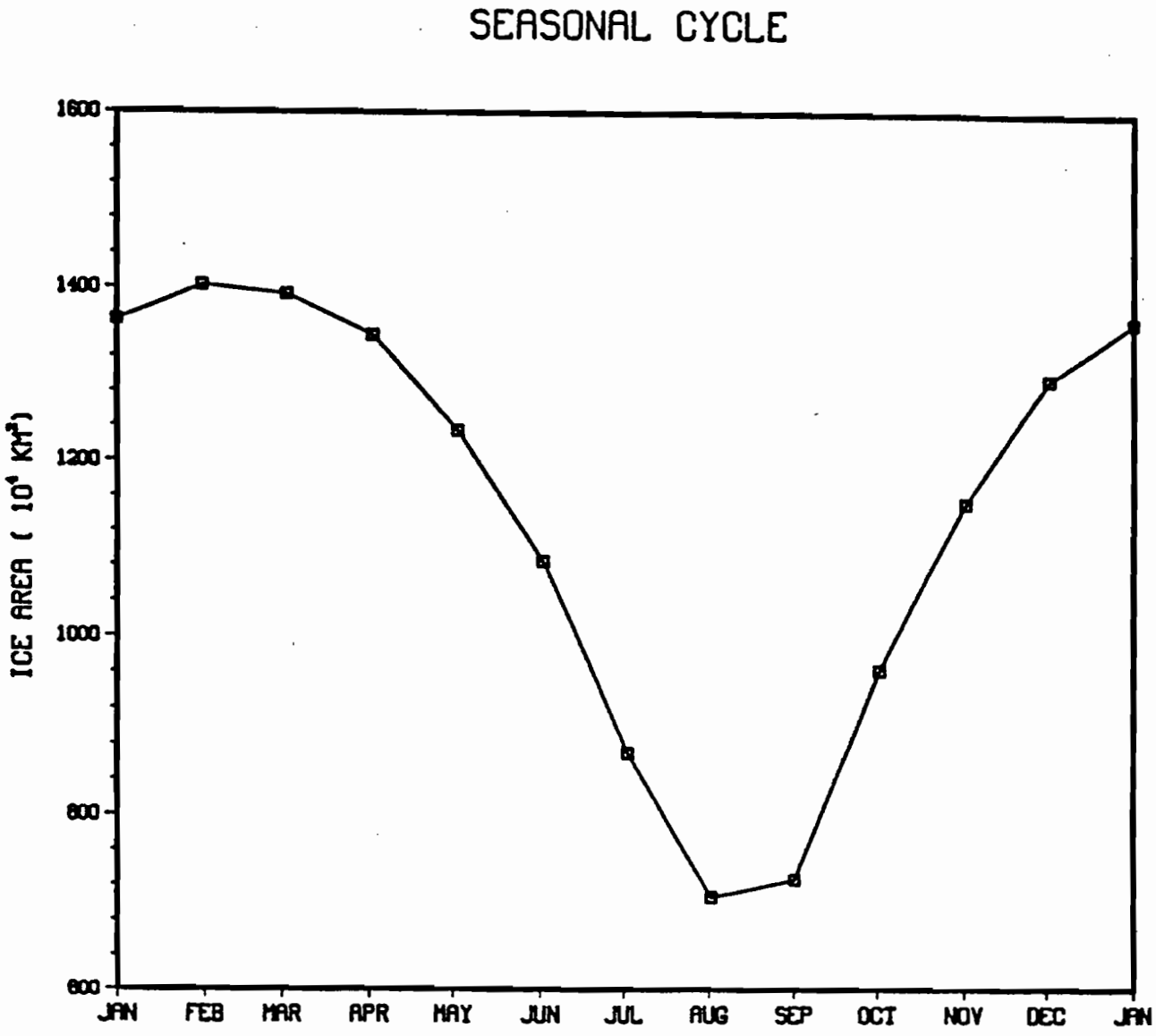

Fig. 9. The normal seasonal cycle of areal sea ice extent in the Arctic.

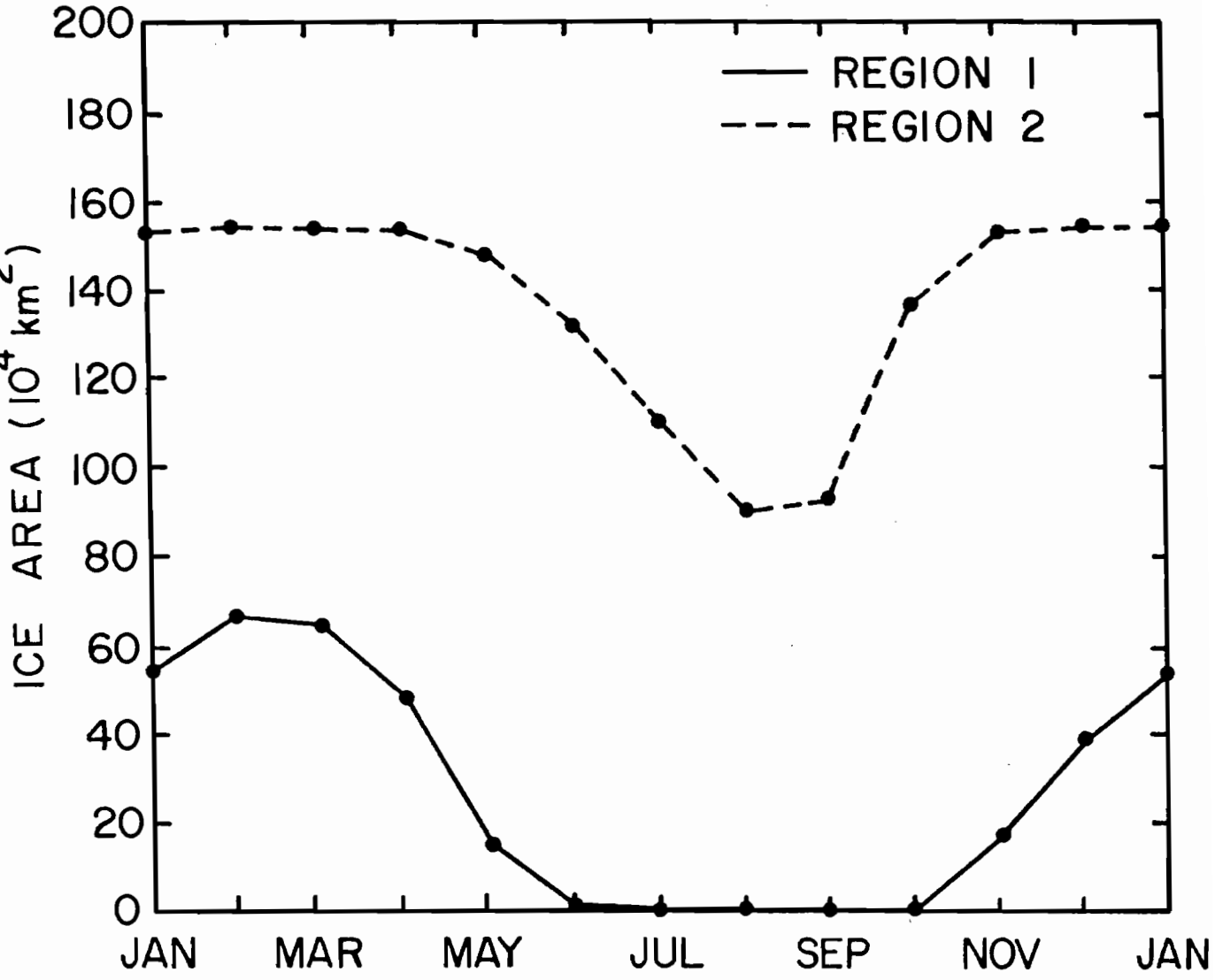

Fig. 10. Seasonal cycles of areal sea ice extent in the Bering Sea (region 1) and the Beaufort & Chukchi Seas (region 2).

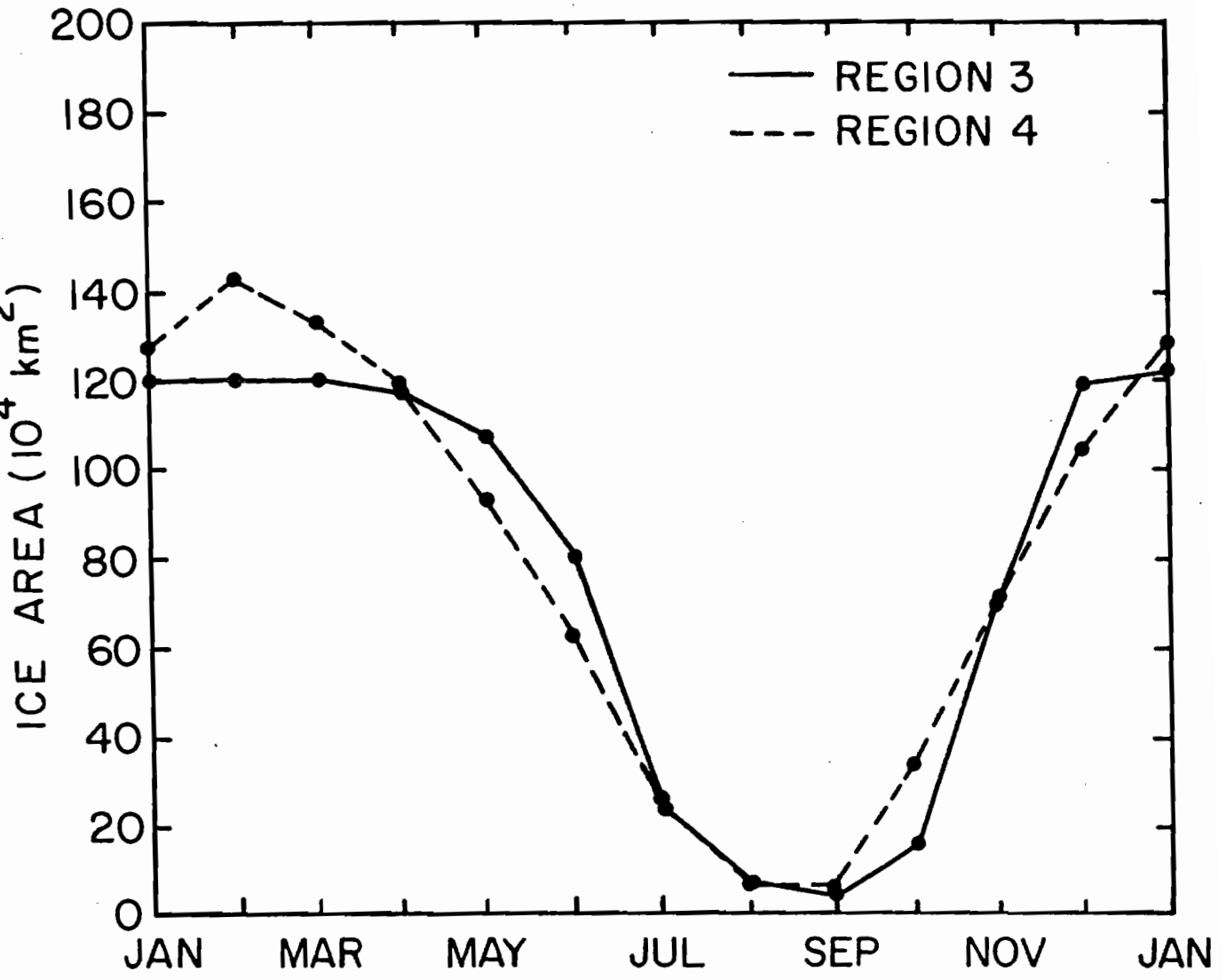

Fig. 11. Seasonal cycles of areal sea ice extent in Hudson Bay (region 3) and the Baffin Bay/Labrador Sea (region 4).

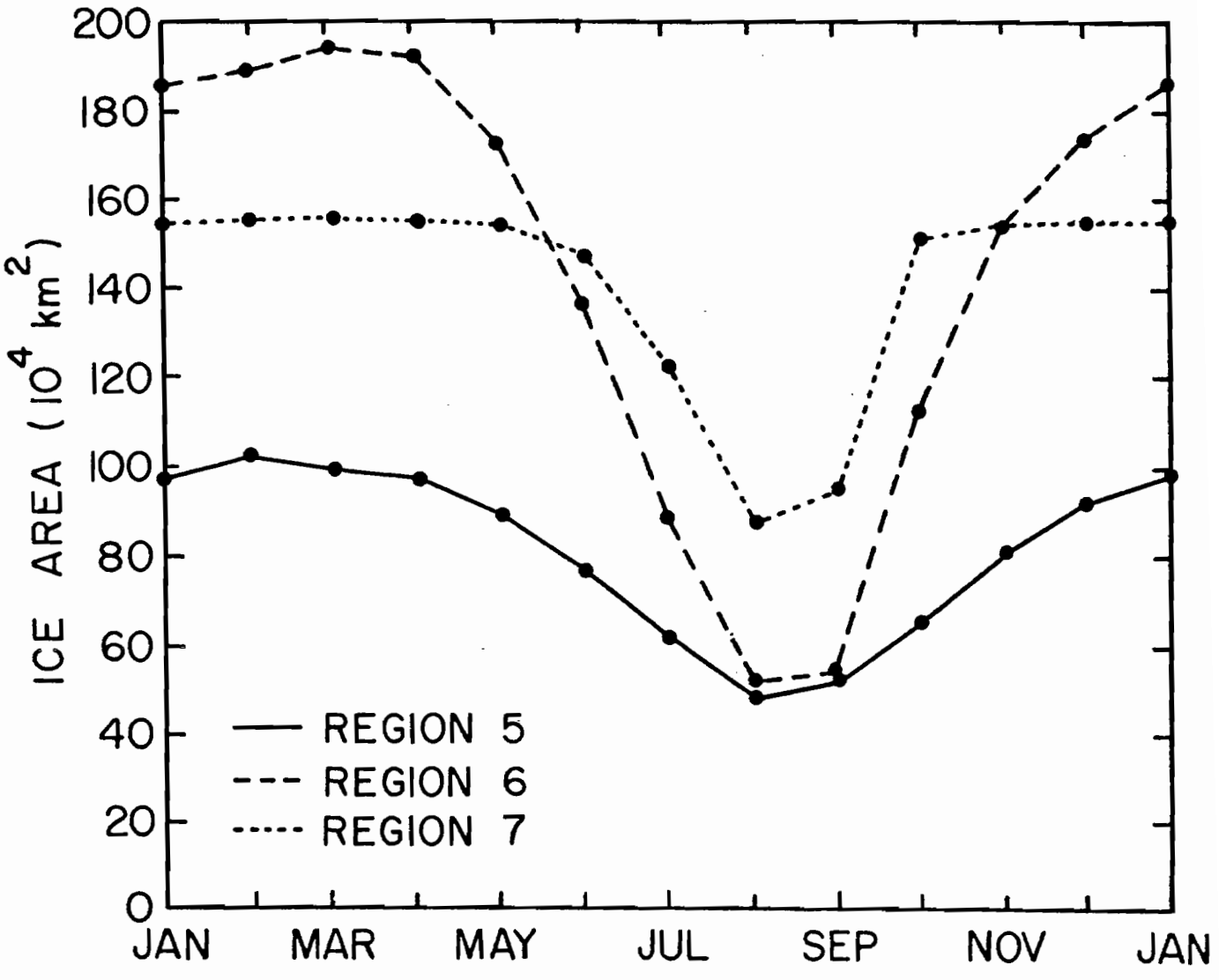

Fig. 12. Seasonal cycles of areal sea ice extent in the Greenland Sea (region 5), the Barents & Kara Seas (region 6) and the East Siberian & Laptev Seas (region 7).

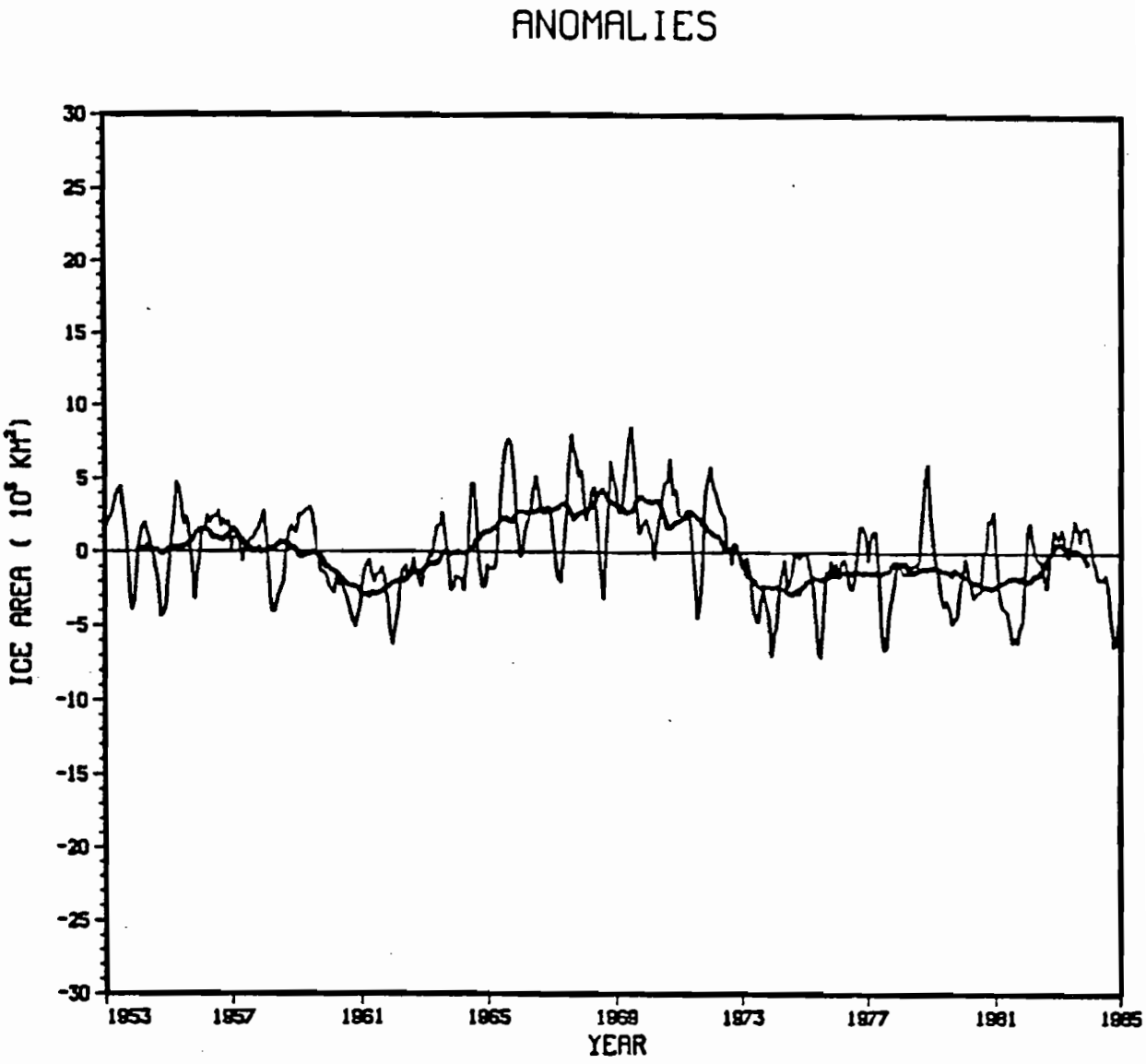

Fig. 13. Smoothed time series of monthly anomalies of areal sea ice extent in the Arctic region. Light and dark curves correspond to 3-month and 25-month running means respectively.

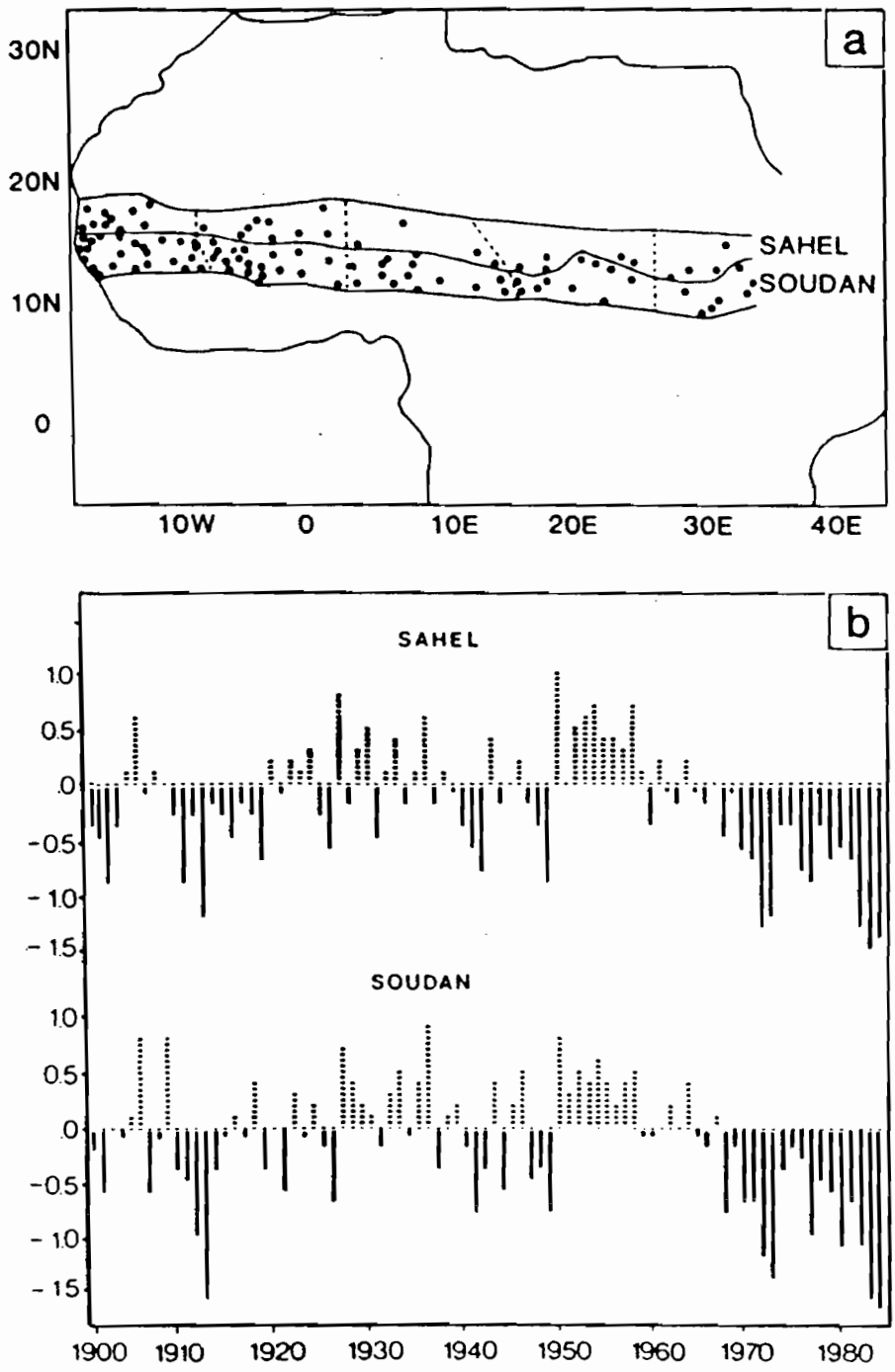

Fig. 14. (a) Station network and location of rainfall zones.
(b) Standardized annual rainfall index for the Sahel and Soudan zones of sub-Saharan Africa. (From Nicholson, 1985.)

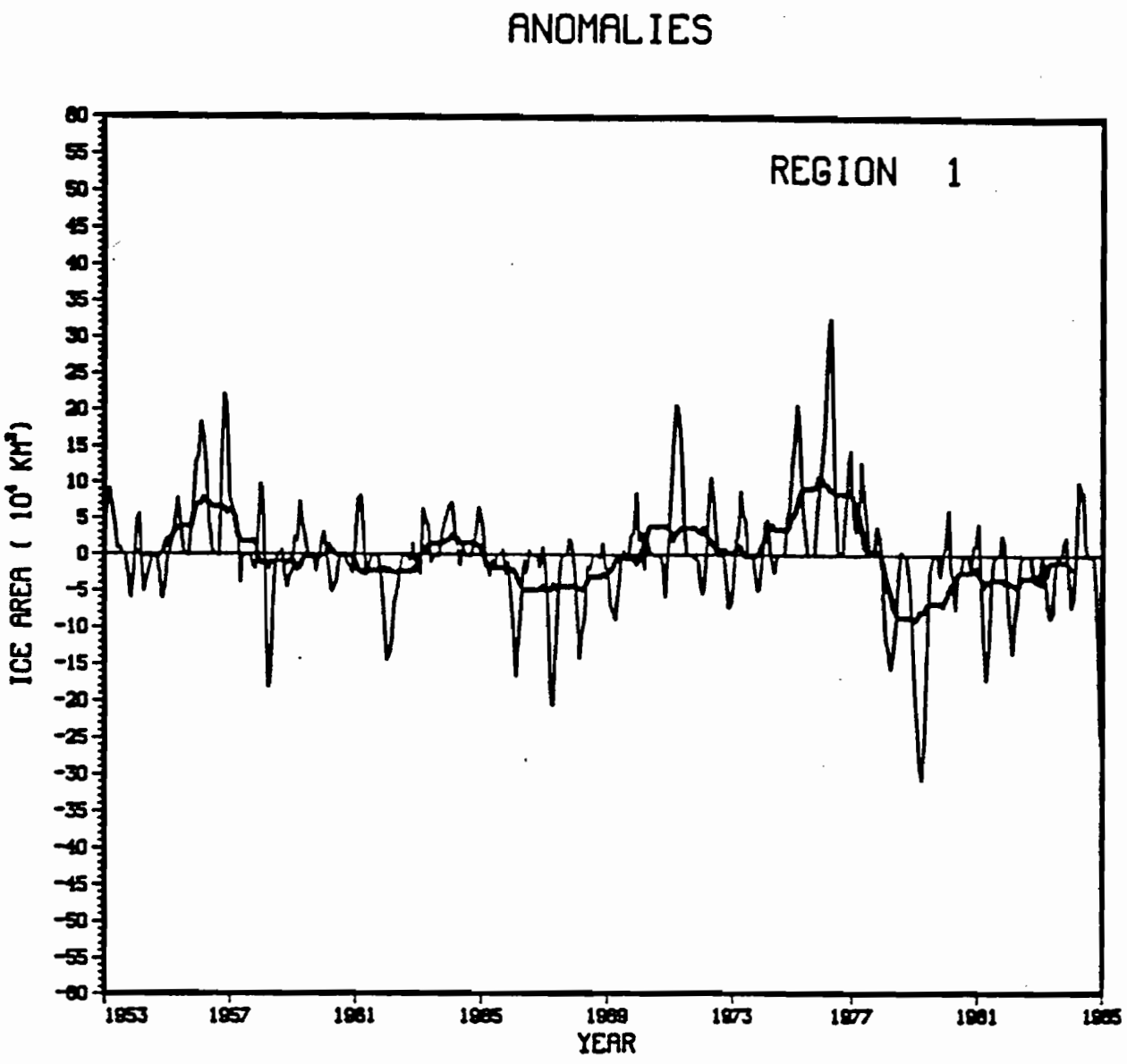

Fig. 15. Same as Fig. 13 except for Bering Sea.

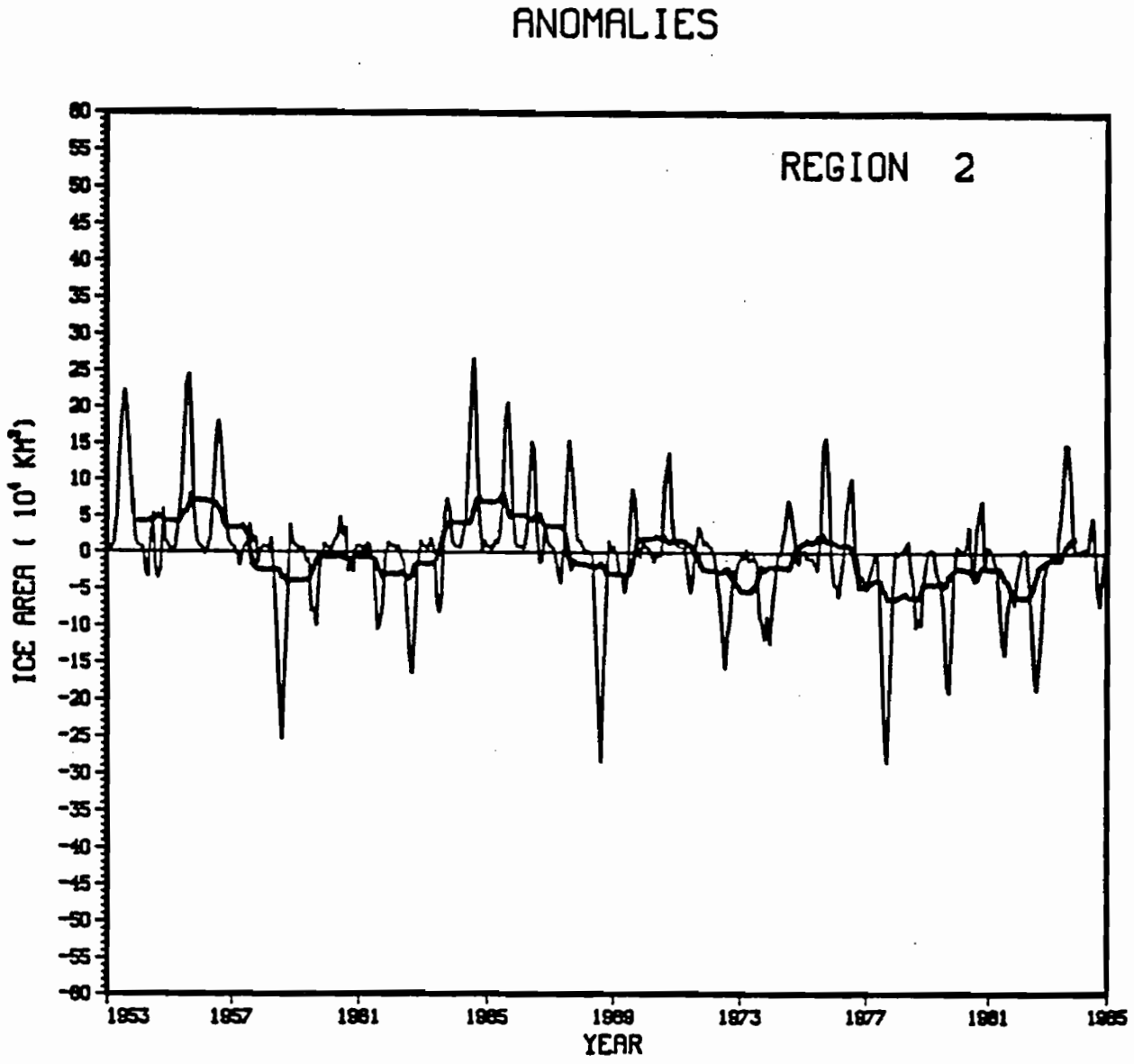

Fig. 16. Same as Fig. 13 except for Beaufort & Chukchi Seas.

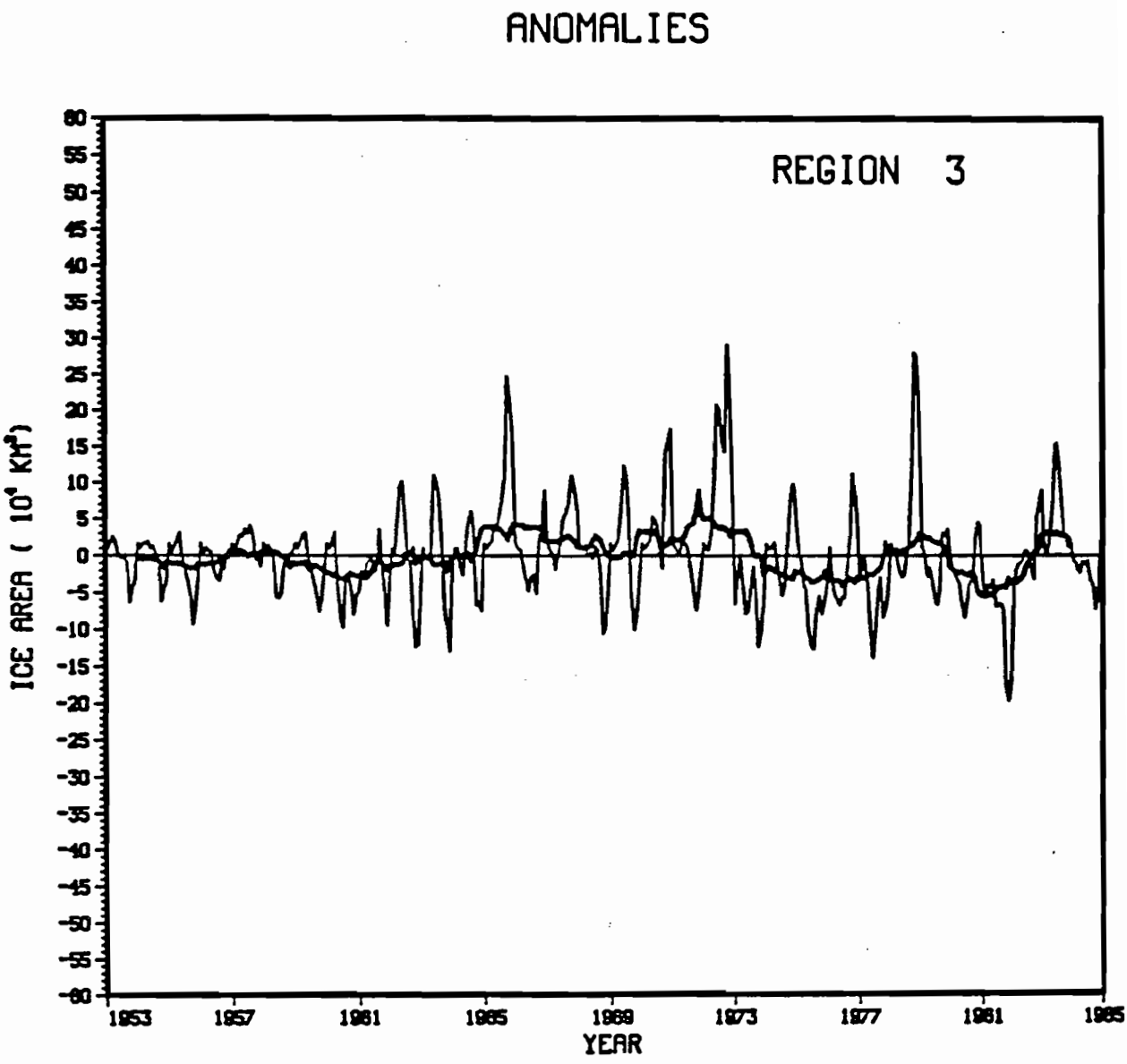

Fig. 17. Same as Fig. 13 except for Hudson Bay.

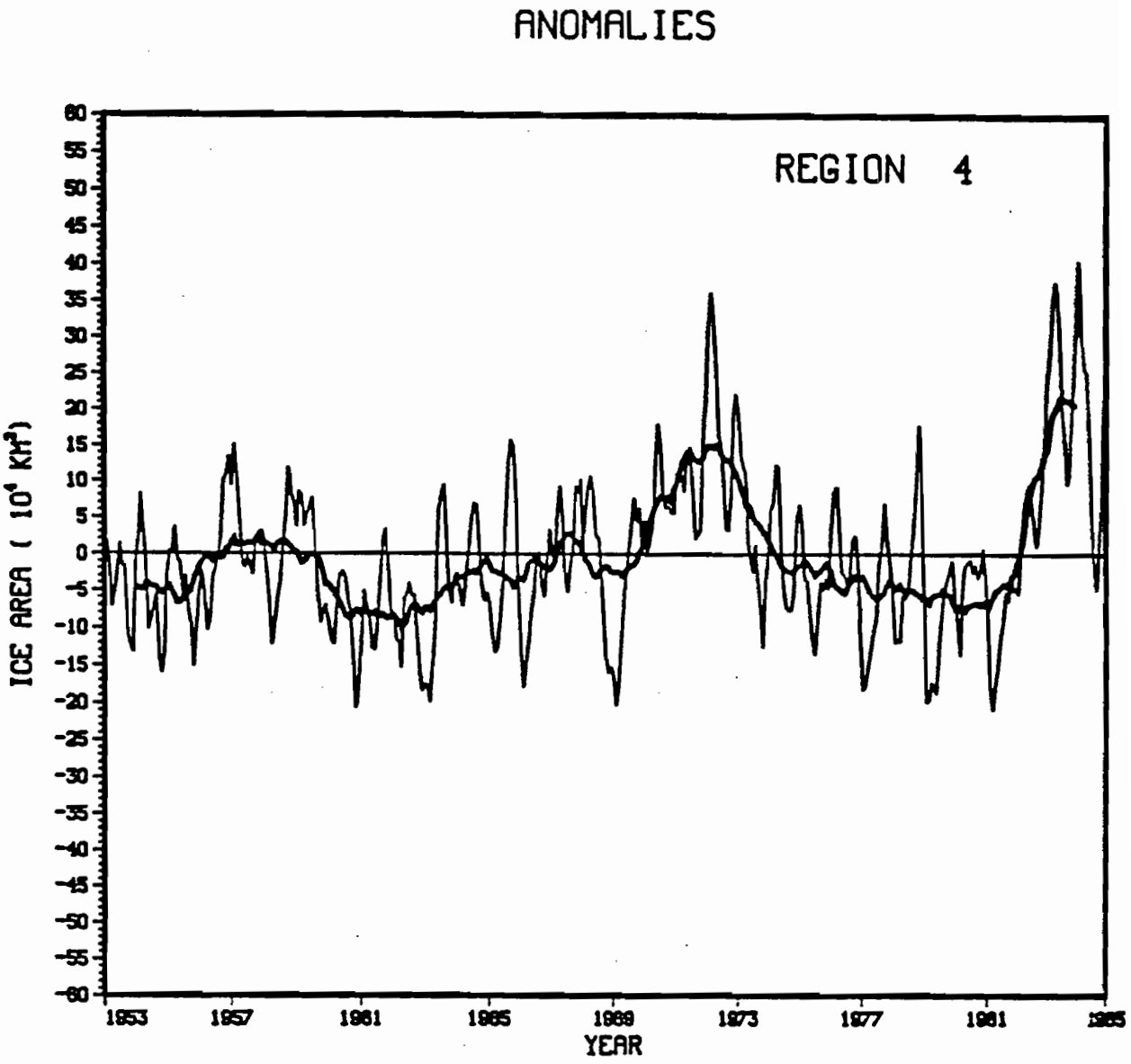

Fig. 18. Same as Fig. 13 except for Baffin Bay/Labrador Sea.

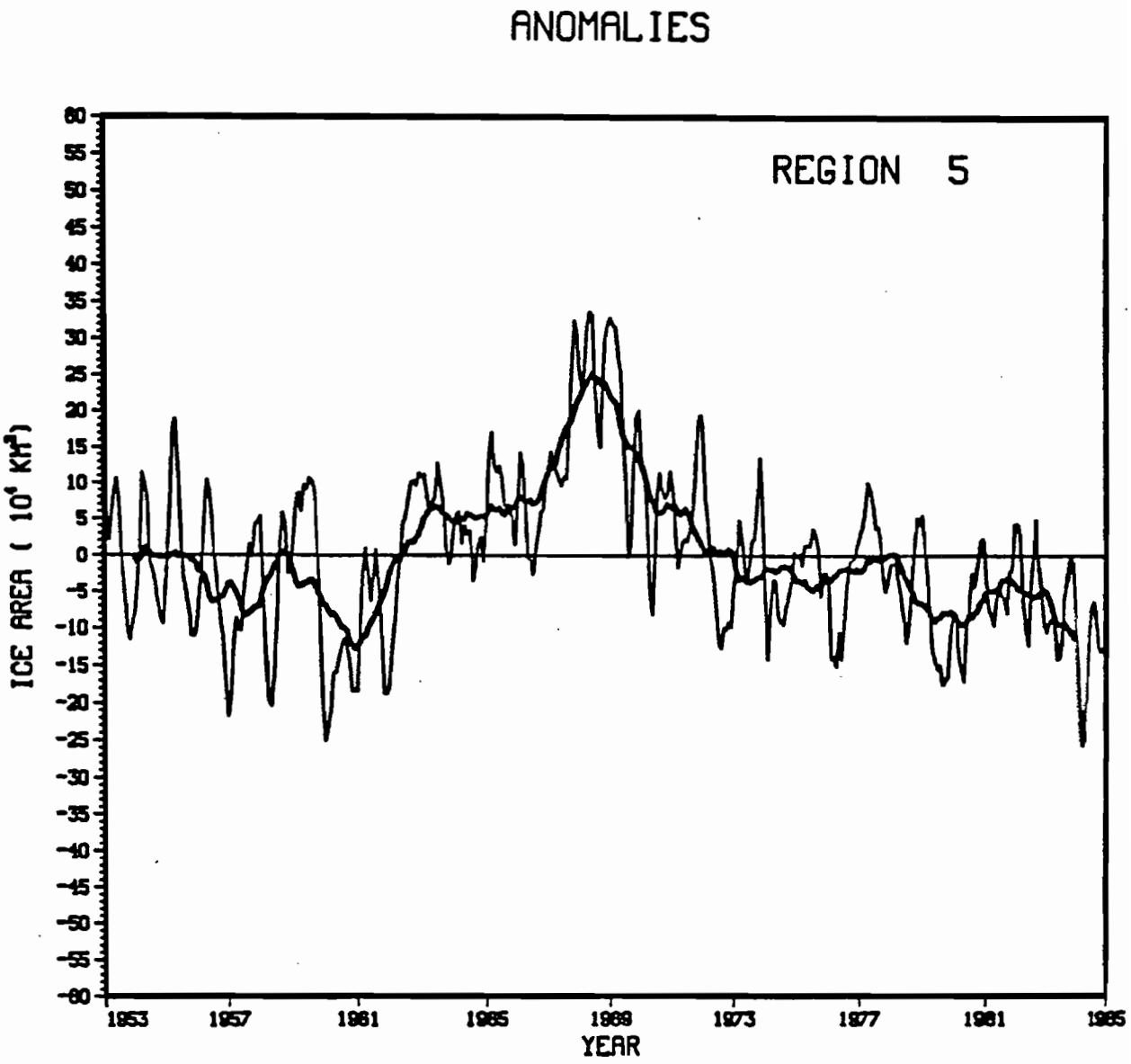

Fig. 19. Same as Fig. 13 except for Greenland Sea.

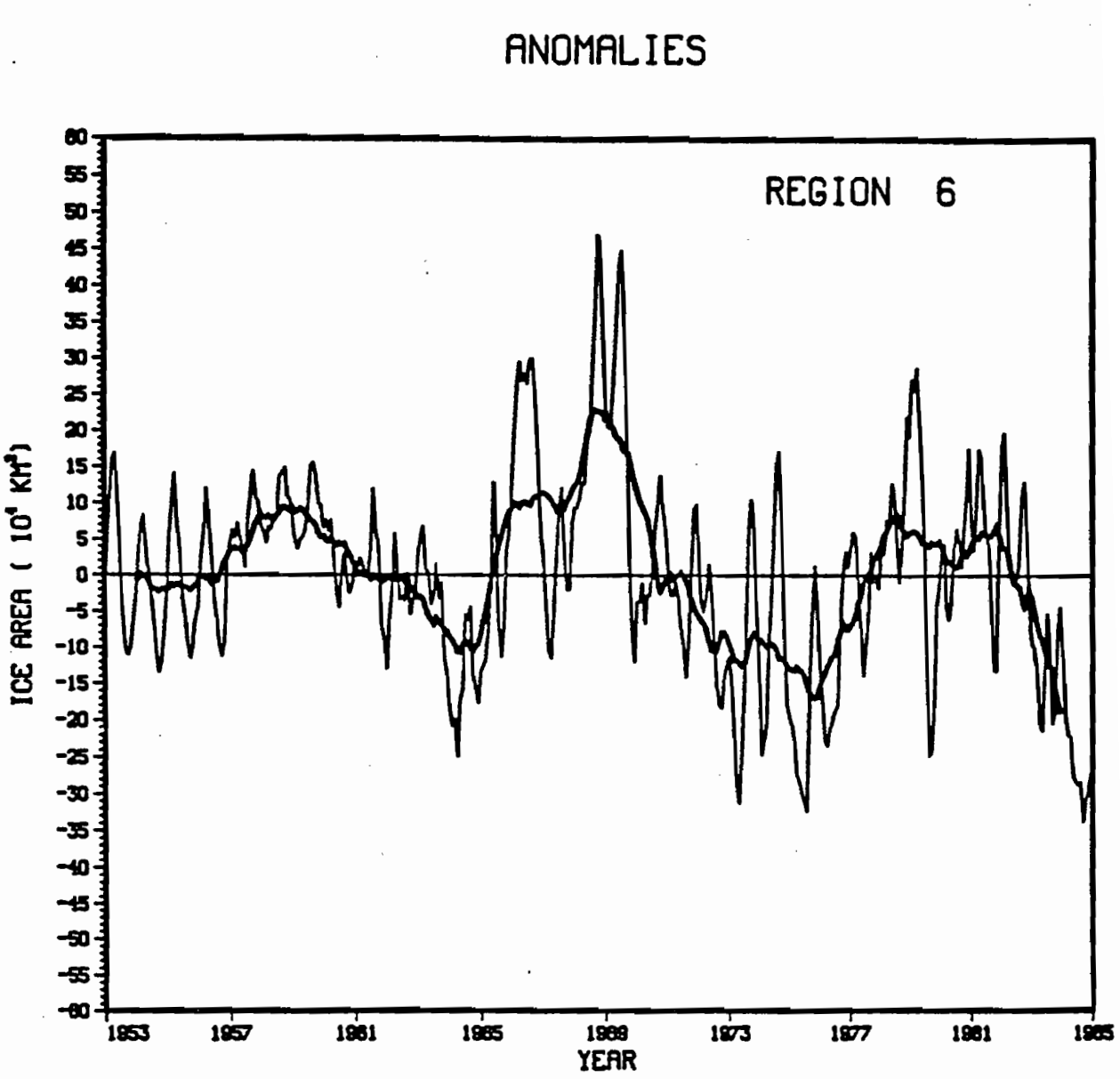

Fig. 20. Same as Fig. 13 except for Barents & Kara Seas.

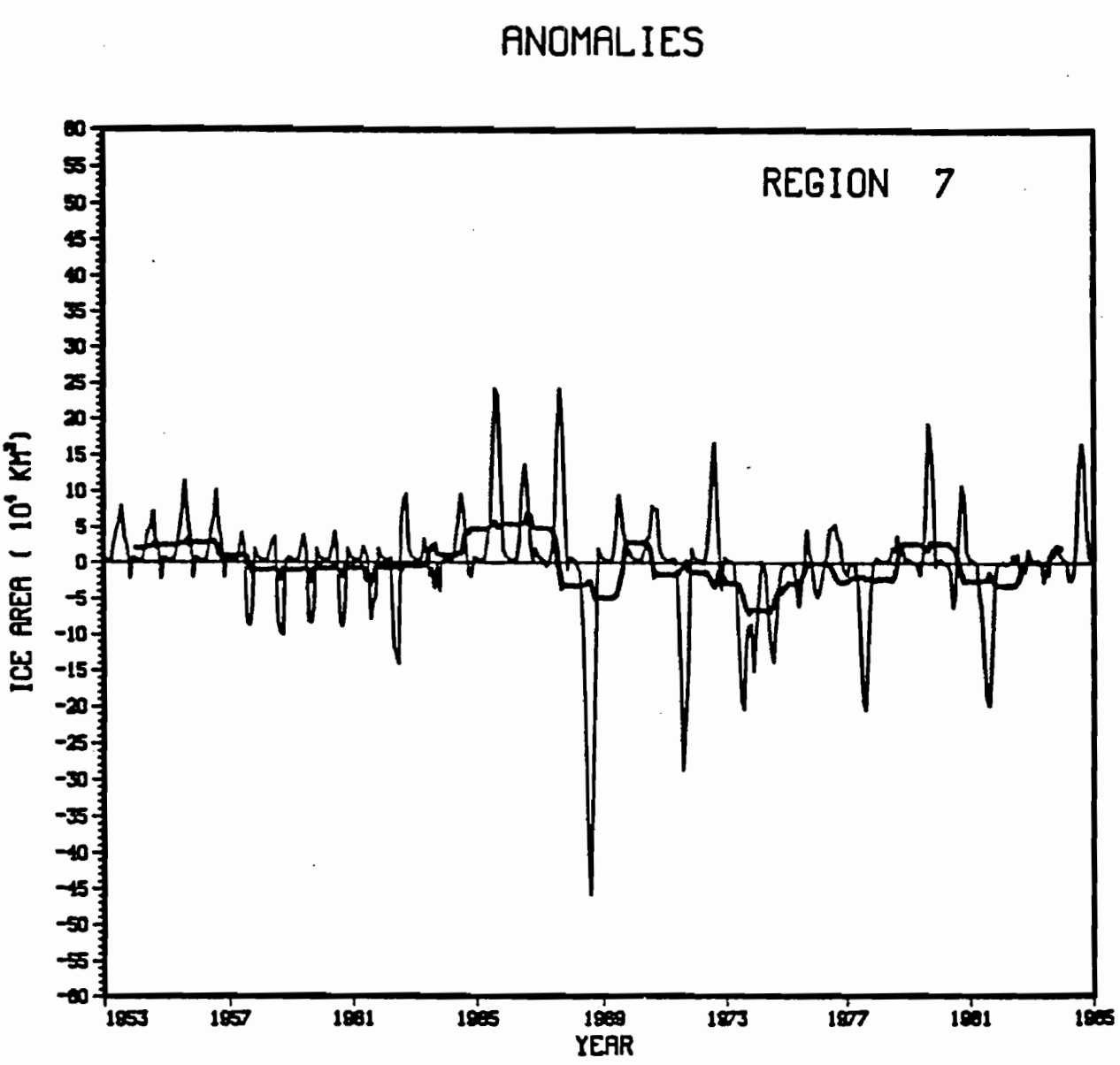

Fig. 21. Same as Fig. 13 except for East Siberian & Laptev Seas.

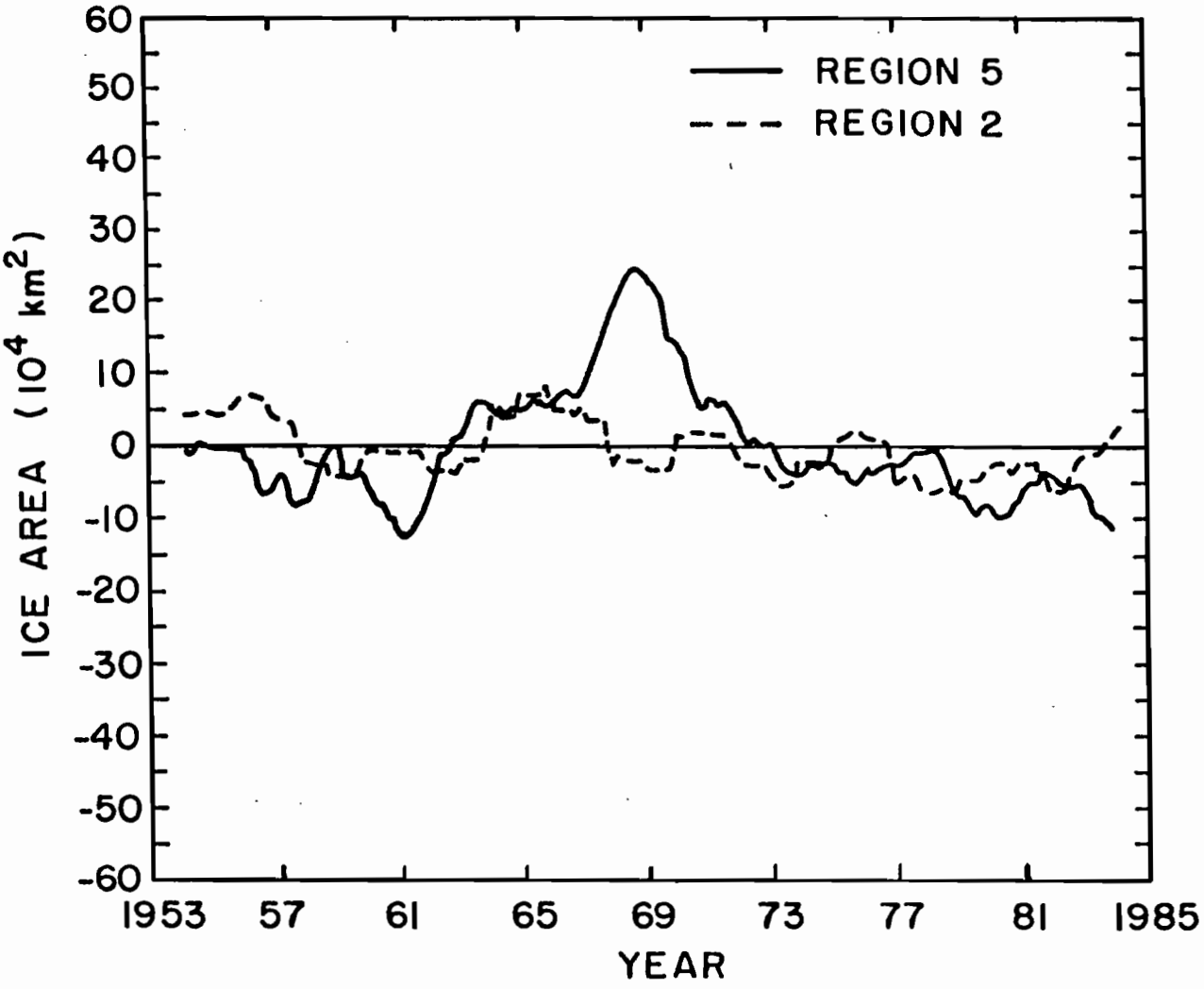

Fig. 22. Superposition of the 25-month smoothed anomalies of areal sea ice extent in the Beaufort (region 2) and Greenland (region 5) Seas.

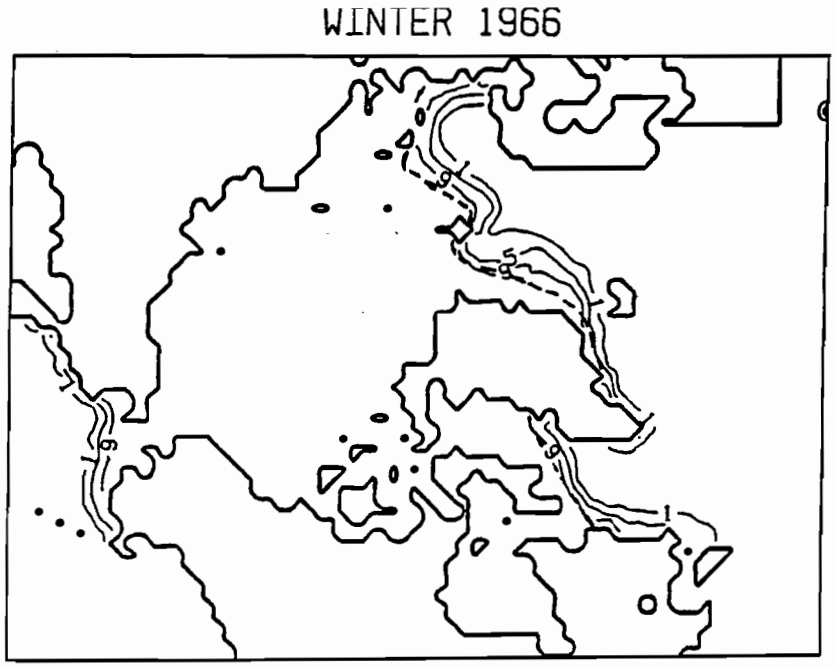

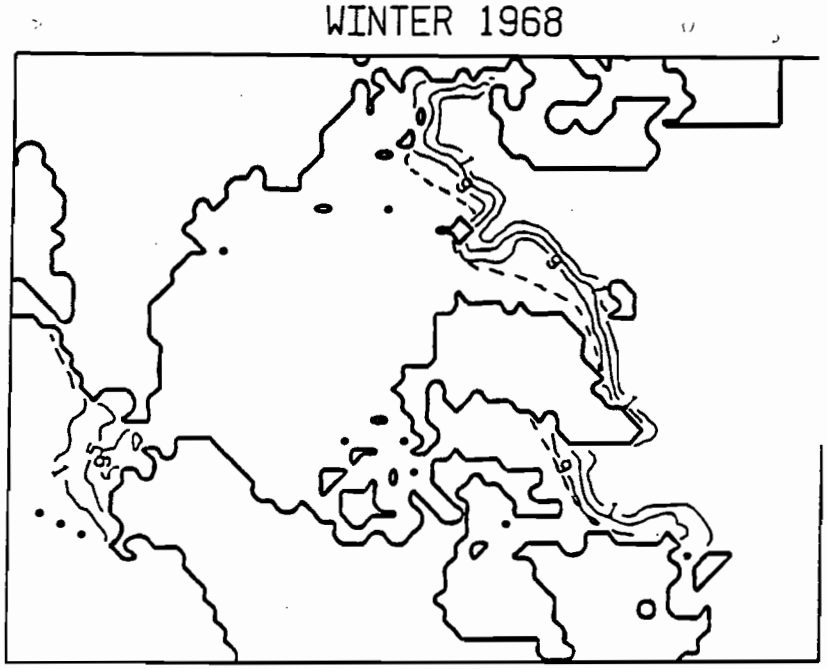

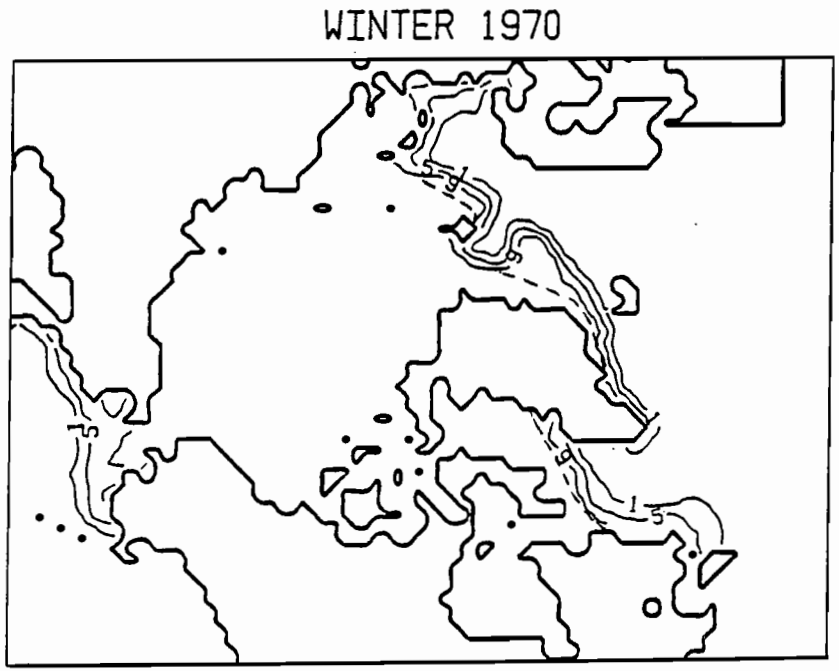

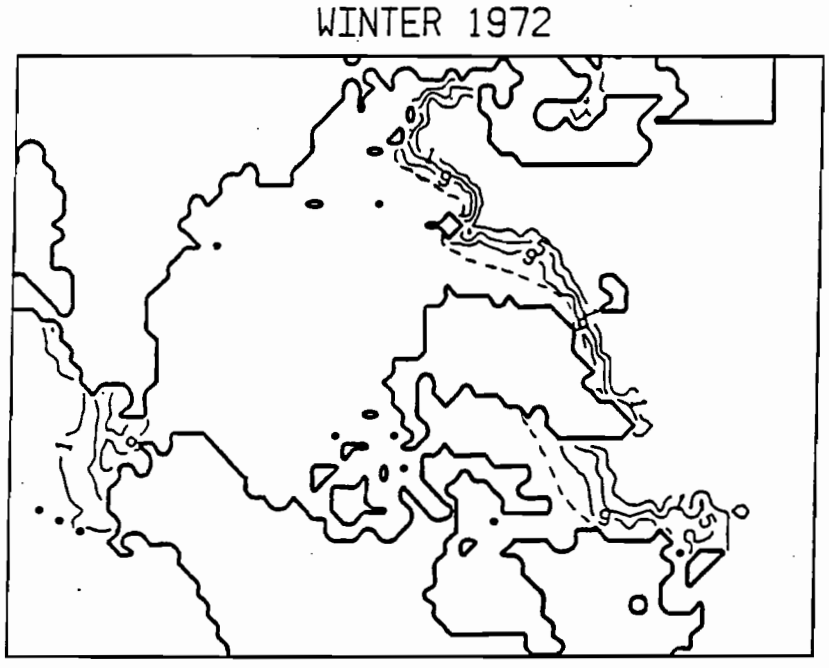

Fig. 23. Bi-yearly sequence of winter maps of sea ice extent from 1966 to 1972. The dashed line (e.g., in the Barents and Greenland Seas) corresponds to the 9/10 contour on the winter climatology map (see Fig. 5).

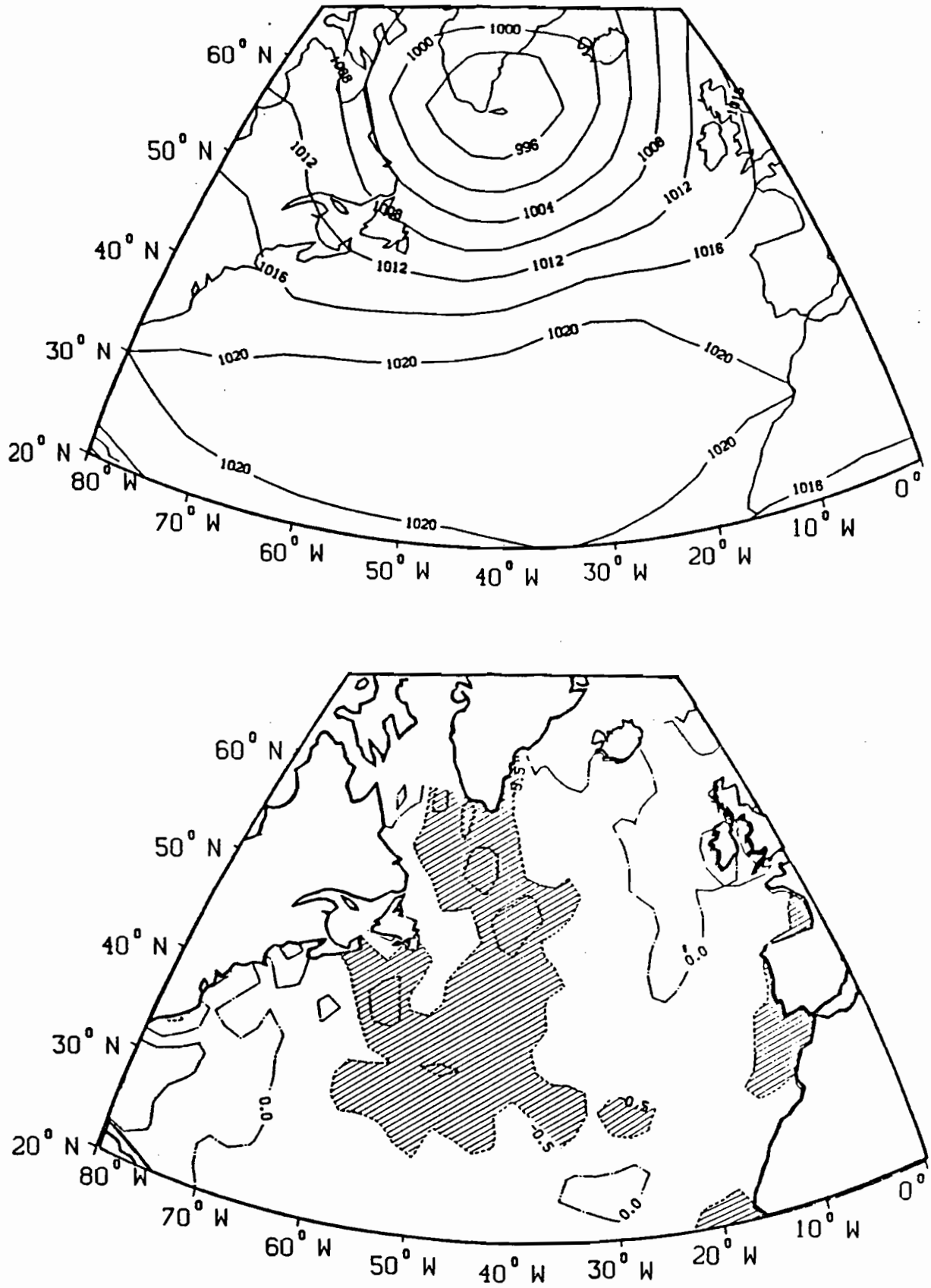

Fig. 24. Maps of North Atlantic sea level pressure (top, in mb) and sea surface temperature anomaly (SSTA) (bottom, in °C) for winter (DJF) 1972. The SST anomalies represent the deviations of temperature from a 1946-79 climatology. (From Allingham et al,m 1987.)

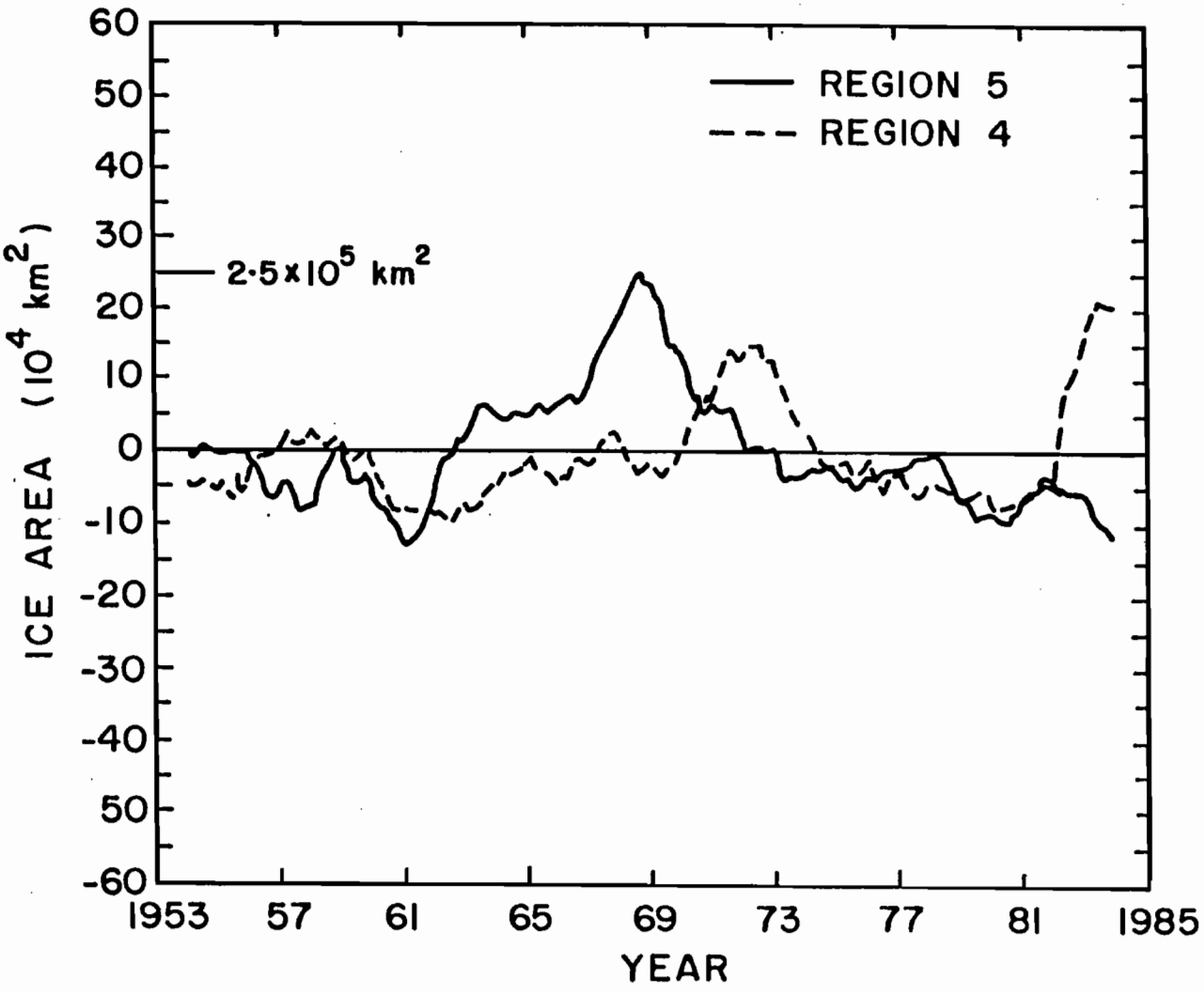

Fig. 25. Superposition of the 25-month smoothed anomalies of areal sea ice extent in the Greenland (region 5) and Labrador (region 4) Seas.